Available online at www.sciencedirect.com
SCIENCE DIRECT®
ELSEVIER
Physica D 184 (2003) 192–225
PHYSICA D
www.elsevier.com/locate/physd

Whip waves

Tyler McMillen [a], Alain Goriely [b,*]

[a] *Program in Applied Mathematics, University of Arizona, Building #89, Tucson, AZ 85721, USA*
[b] *Department of Mathematics, University of Arizona, Building #89, Tucson, AZ 85721, USA*

Abstract

The sound created by a whip as it cracks is produced by a mini-sonic boom created by a supersonic motion of the end of the whip. To create such a motion, one sends an impulse to the handle of the whip that travels to the end and accelerates the tip to supersonic speed. The impulse which creates a whip crack is studied as a wave travelling along an elastic rod. The whip is modeled as an inextensible, unshearable, inhomogeneous planar elastic rod. A crack is produced when a section of the whip breaks the sound barrier. We show by asymptotic analysis that a wave travelling along the whip increases its speed as the radius decreases—as the whip tapers. A numerical scheme adapted to account for the varying cross-section and realistic boundary conditions is presented, and results of several numerical experiments are reported and compared to theoretical predictions. Finally, we describe the shape of the shock waves emitted by a material point on the whip travelling faster than the speed of sound.

PACS: 46.70.Hg; 46.40.−f; 05.45.−a

Keywords: Travelling waves; Inhomogeneous; Shock waves; Mach cone; Whips; Elastic rods

1. Introduction

Whips are rather unique objects. Most whips have been developed for the sole purpose of producing a sharp distinct loud noise, the well-known crack. The physical origin of this sound is a common physics trivia question whose correct answer is, surprisingly, known by many people. The crack of a whip is a mini-sonic boom, not unlike the sound of a supersonic bullet, created when the tip of the whip travels faster than the speed of sound. This simple fact leads naturally to a second question: how does the tip of a whip get accelerated to supersonic velocities? The initial impulse given to a whip is of moderate velocity, usually less than a tenth of the speed of sound, and within a few meters this impulse moves to velocities two or three times larger than the speed of sound. Experimental observations (see below) indicate acceleration in excess of 50,000 times the acceleration of gravity. What are the physical ingredients necessary to produce such a tremendous acceleration? In this paper we address these questions in the context of wave dynamics propagating on elastic rods.

There are two different types of whips. The whips we are studying are long, tapered, and single-threaded whips such as the bullwhip, coachwhip, and snakewhip used to produce cracking noises and not the whips used

* Corresponding author. Tel.: +1-520-621-2559.
E-mail addresses: mcmillen@math.arizona.edu (T. McMillen), goriely@math.arizona.edu (A. Goriely).

0167-2789/$ – see front matter © 2003 Elsevier B.V. All rights reserved.
doi:10.1016/S0167-2789(03)00221-5

for torture and other perverse activities which are short, bulky, knotty and multi-threaded such as the infamous "cat-o'-nine-tails", and generally of no apparent scientific interest. The origin of noise-making whips is lost in history as they seem to have been used by early farming communities to direct cattle and horses by various cultures around the world. The main modern development of whip technology is associated with the European conquest of the American West and Australia where small whips with short handles were needed for open ranching. Nowadays, the whip has lost most of its commercial use despite having become a mythical object for Hollywood entertainment at the hands of Xena, Indiana Jones, and Zorro. The art of the whip is kept alive by a few dedicated craftspeople and whip enthusiasts (more general references about whips can be found in books and videotapes [1–3]). At a scientific level, whips with their association to perverse activities and entertainment use, have not received much attention and only a handful of theoretical and experimental works have been performed (see [4] for a complete historical account). Shortly after Mach's ballistic experiments in the 1880s, it was recognized by Otto Lummer in 1905 that the crack of a whip is also a sonic boom, created when a section of the whip travels faster than the speed of sound [5]. Despite some early confusion and discussions about the origin of the crack (early letter exchanges in Scientific American are particularly interesting [6–9]), Lummer's hypothesis was generally accepted by mainstream scientists such as Prandtl [10], Boys [46], and Bragg [11]. Lummer's insight was finally proved experimentally by Carrière in 1927 [12,13] who showed through high-speed shadow photography that a sonic boom is indeed created by the whip wave and recorded tip velocities in excess of 900 m/s (the typical speed of sound in the air is around 330 m/s). Further observations were recorded by Bernstein et al. in 1958 [14] and more recently in 1998, in a beautiful high-tech, high-speed digital photography experiment by Krehl et al. [4] where acceleration of up to $50{,}000 \times g$ was recorded (Fig. 1). In the latter two cases, the authors only report the observations of a real bullwhip manipulated by a circus performer (as opposed to the experiments of Carrière performed with a "laboratory" whip under controlled acceleration and tension). Moreover, Krehl et al. report the following counter-intuitive observation: a sonic boom is emitted when the tip velocity reaches about *twice* the speed of sound in air.

Previous theoretical studies on the dynamics of whips have reached seemingly mutually exclusive, contradictory results, with no apparent reconciliation in the literature. Most of these formulations involved posing the propagation of a whip wave as a one-dimensional energy problem [16–18]. Naively, as a wave travels down a whip, the mass that is travelling decreases. Thus, in order to maintain energy conservation, the speed must increase. This leads, however, to some non-intuitive results, such as the speed of the tip approaching infinity [14]. On the other hand, Steiner and Troger [19] have shown that if linear momentum is conserved for an assumed shape, then the speed of the tip remains constant. The singularity formed at the free-end of a string when the wave reaches the end was also studied by Zak et al. [20]. The speed of the tip of a whip does accelerate as the wave travels down the length of the whip, but it does not approach infinity, even if it does taper to zero radius. Furthermore, whips made of rods with

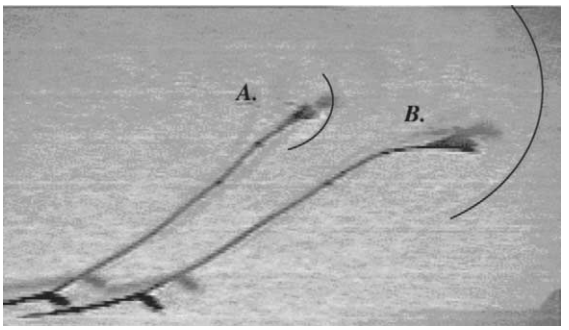

Fig. 1. High-speed digital shadow graphs of a cracking whip and its sonic boom. The time interval between the two pictures is 111 μs. The solid lines are superimposed over the shock waves. The velocity at the time of the crack was Mach 2.19. Picture courtesy of Krehl et al. [4].

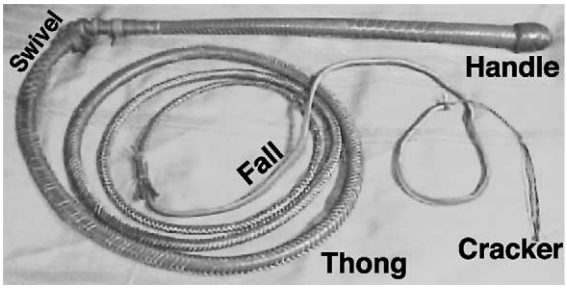

Fig. 2. An 8 ft Australian stockwhip.

constant cross-section can also be made to crack, discounting the hypothesis that tapering alone can account for the phenomenon. These formulations, while interesting, suffer all from the same flaw, which is the failure to account for the shape of the whip. One cannot simply assume the shape in space of the whip and solve for the velocity; it obeys physical laws that are coupled to the dynamics. We present in this paper a model where energy, linear and angular momenta are conserved in the whip wave, and show that the speed of the tip accelerates as the wave reaches the end of the rod, but that its maximum speed is indeed finite, and the acceleration is related to the tapering, length and physical characteristics of the rod. However, before we proceed with our analysis, we must understand the true characteristics of whips and how they are actually handled.

Most whips have three main components (see Fig. 2). The first part of the whip is the handle, generally made of wood and ending with a connection to the thong, sometime with a swivel. It is designed to control the second and main part of the whip, the thong, a long, tapered, finely braided section made of quality leather (kangaroo preferred). The last important part of the whip is the cracker, a small piece of string that produces the cracking sound and takes most of the abuse. It is made so that it can easily be replaced after a few hundred cracks. The typical whips used by coachmen and coach-women for horse training and control have a long handle which is about the same length as the thong itself. There are fairly easy to crack as the handle provides a huge lever to accelerate the initial impulse. Snakewhips and bullwhips were developed so that they can be carried in a saddle, they have a short handle and require practice and dexterity but also allow for a variety of cracks.

How does one crack a whip? Whips can be dangerous for their users. The long thong and cracker under untrained hands can easily lash back at one's face or rip one's pants leaving embarrassing scars. There are two main ways to crack a whip. When given a whip most people will try to move it up and down (Fig. 3). This so-called *downward*

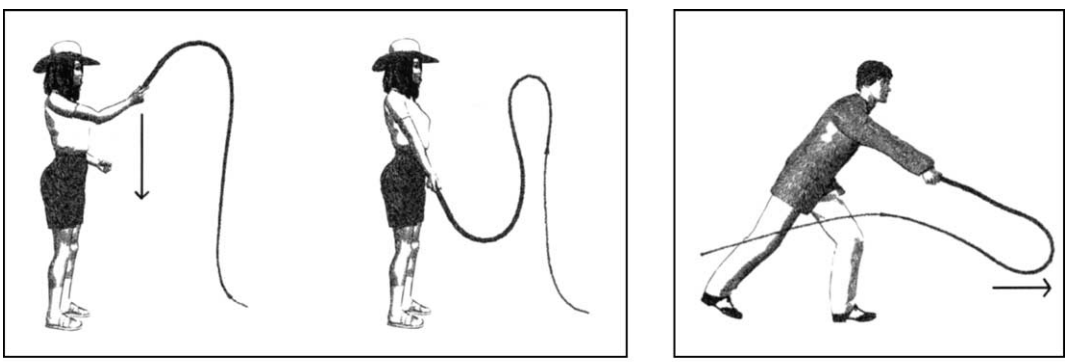

Fig. 3. The downward snap and a variation, the underhand snap (drawing courtesy of Conway [21]).

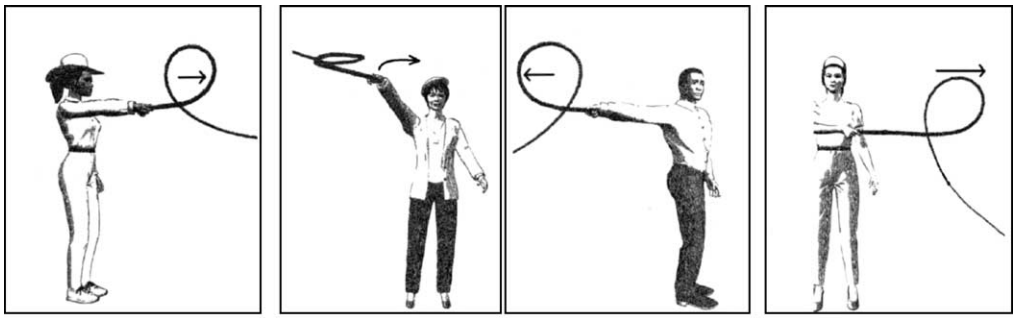

Fig. 4. (A) The forward crack and variations, (B) the overhead crack, (C) the reverse crack and (D) the figure-eight crack (drawing courtesy of Conway [21]).

snap can be carried along different directions and requires sufficient acceleration of the handle to create an efficient crack. Notice that since the handle is moved during the entire process, work is performed and the energy is not conserved. This rather intuitive way to crack a whip is not the type of motion privileged by professionals. The most efficient way to crack a whip, the so-called *forward crack*, is to move the handle as to create a loop in the whip that travels to the end of the whip. The same type of crack can be achieved in different planes and direction (see Fig. 4). The key feature that we will use for our analysis is the propagation of a loop along a tapered rod with one end with controlled tension (the handle) and one free end (the tip).

In analyzing this phenomenon, we study the whip in the context of elastic rods in which the problem can be posed as one of a wave travelling in an inhomogeneous medium (the inhomogeneity being provided by the tapering). The propagation of waves along an inhomogeneous background has been a topic of study in several fields [22–28], the simplest one being the propagation of a water waves arriving at shore where depth varies. In this context, the analysis of soliton equations such as Korteweg–de Vries and the nonlinear Schrödinger equations have become paradigmatic. The idea is to study the propagation of solitons in the presence of slowly varying parameters to model slow changes in the background. Here we study a similar but different problem: the propagation of waves along an elastic rod in the plane for which the radius varies along its length. We begin with a known travelling loop solution travelling along an ideal infinite rod. An asymptotic analysis shows that the speed of this travelling wave increases if the radius of the rod decreases. Numerical analysis is performed to examine the behavior of the rod as the solitary shape reaches the end of the rod, when the crack is produced. Propagation of similar loops are found in fly-fishing [29,30] and in sperm motility [31] (albeit in a highly viscous material where the model proposed here will not apply). Finally, in recent years, it has been suggested that the tapered tail of apatosorus might have been used as a giant whip and simulations on the motion of chains based on archeological data shows that part of the tail could have exceeded the speed of sound in the air [15].

This paper is organized as follows. First, we derive the equations governing planar elastic rods with a varying cross-sectional area. Then, we examine conservation laws and travelling wave solutions to these equations. We examine how the wave travels when it is far from the end of the rod, and can be approximated by a wave travelling on an ideal infinite rod. In this context we examine how the speed of a travelling wave is affected by the tapering of the rod. Second, we turn to the behavior of the wave as it reaches the end of the rod, and rapid acceleration occurs to create a shock. A dedicated numerical scheme for the rod equations with constant radius and periodic boundary conditions is modified to take account of the varying radius and different types of boundary conditions. We calculate numerically the maximum speed of the tip, and how it is related to the tapering and the tension applied at the handle. Third, we examine the shape of a shock wave emitted from an object travelling in an arbitrary path at

greater than the speed of sound, and apply this to determine the shock waves emitted from the tip of a whip as it is cracked.

2. Assumptions and governing equations

We model a whip as an elastic rod [32,33]. Most whips are made from leather, whose elastic constants are known [34]. However, whips can be made from such mundane items such as strings, cotton ropes, or even wet towels [35]. In any case, the materials that various whips are made from can all be reasonably modeled as elastic rods. The most efficient means of cracking a whip involve sending a planar loop (Fig. 4) down the whip, so we assume that the rod lies in the Euclidean x–y plane, and since the same crack can be performed in vertical or horizontal planes we neglect the effect of gravity. We also assume that the rod: (i) has circular cross-sections with varying radius $R(s)$, (ii) is inextensible, (iii) is unshearable, (iv) obeys a linear constitutive relationship and, (v) the properties of the material, such as the density and elastic properties, are constant. We neglect in our analysis the effect of air friction. This effect is crucial to understand the formation of a sonic boom but not for the acceleration of the loop itself.

Let $(\mathbf{e}_x, \mathbf{e}_y, \mathbf{e}_z)$ be a fixed orthonormal basis in the Euclidean space and let $\mathbf{r}(s,t) = x\mathbf{e}_x + y\mathbf{e}_y \equiv (x(s,t), y(s,t))$ be the centerline of the rod in the x–y plane, where s is the arc-length and t is time. The tangent vector $\mathbf{t}$ is given by

$$\mathbf{t} = \frac{\partial \mathbf{r}}{\partial s} = t_x\mathbf{e}_x + t_y\mathbf{e}_y. \tag{1}$$

We define the angle φ (see Fig. 5) to be the angle between $\mathbf{e}_x$ and $\mathbf{t}$ so that

$$t_x = \cos(\varphi), \tag{2}$$

$$t_y = \sin(\varphi). \tag{3}$$

From Frenet's equations [36], we have that $\mathbf{t}' = \kappa\mathbf{n}$, where $\mathbf{n}$ is the normal to the curve $\mathbf{r}$ and κ is the curvature so that $\kappa = \varphi'$. (Here $(\cdot)'$ denotes differentiation with respect to the arc-length s, and we will denote by $\dot{(\cdot)}$ differentiation with respect to time t.) We call the force and moment $\mathbf{F} = F\mathbf{e}_x + G\mathbf{e}_y$ and $\mathbf{M}$, respectively. The balance of linear momentum gives

$$\rho A\ddot{x} = F', \tag{4}$$

$$\rho A\ddot{y} = G', \tag{5}$$

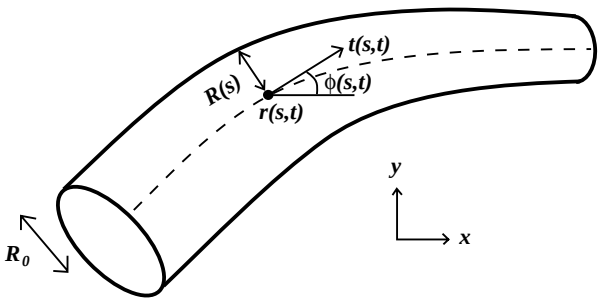

Fig. 5. A rod in the plane. The centerline of the rod is $\mathbf{r}$.

where ρ is the density per unit volume, and $A = A(s)$ is the cross-section area at the material point s. The linear constitutive relationship, relating the moment to the strain κ, is, with $\mathbf{M} = M\mathbf{e}_z$,

$$M = EI\kappa = EI\varphi', \tag{6}$$

where E is the Young's modulus and $I = I(s)$ the moment of inertia of the circular cross-section. The balance of angular momentum generates an equation for φ,

$$\rho I\ddot{\varphi} = (EI\varphi')' + G\cos(\varphi) - F\sin(\varphi). \tag{7}$$

Since the cross-sections are circular, we have

$$A = \pi R^2, \qquad I = \tfrac{1}{4}(\pi R^4), \tag{8}$$

where $R = R(s)$ is the radius of the cross-section. We use the following scaling:

$$t = \frac{R_0}{2}\sqrt{\frac{\rho}{E}}\tilde{t}, \qquad s = \frac{R_0}{2}\tilde{s}, \tag{9}$$

$$\mathbf{r} = \tfrac{1}{2}(R_0)\tilde{\mathbf{r}}, \qquad \mathbf{F} = E\pi R_0^2\tilde{\mathbf{F}}, \tag{10}$$

where $R_0 = R(0)$ is the radius of a cross-section at a given reference point. Notice that, in this scaling, when $\tilde{s} = 1$, $s = R_0/2$, so the radius of the rod in the new variables is 2 at the reference cross-section $R = R_0$. Furthermore, from (7), we see that the speed of sound in the rod is

$$c_{\mathrm{m}} = \sqrt{\frac{E}{\rho}}. \tag{11}$$

To relate the speed of a wave in the new variables to the speed in the original variables we notice that a speed of 1 in the new variables corresponds to $\Delta\tilde{s}/\Delta\tilde{t} = 1$, and that

$$\frac{\Delta s}{\Delta t} = c_{\mathrm{m}}\frac{\Delta\tilde{s}}{\Delta\tilde{t}}, \tag{12}$$

so that a speed of 1 in the scaled variables corresponds to the speed of sound in the material (note that the rod is modeled as being inextensible and therefore sound waves cannot travel in the material. Nevertheless, the value c_{m} still provides the proper scaling for flexural waves). The speed of sound in leather is approximately 220 m/s, comparable to the speed of sound in air, 330 m/s [34].

We define the ratio of the area of the cross-section to the reference cross-sectional area,

$$\delta(s) = \frac{R^2(s)}{R_0^2}. \tag{13}$$

If the radius is constant, $\delta \equiv 1$. Then, the equations become, after scaling and dropping the tildes,

$$\delta\ddot{x} = F', \tag{14}$$

$$\delta\ddot{y} = G', \tag{15}$$

$$\delta^2\ddot{\varphi} = (\delta^2\varphi')' + G\cos\varphi - F\sin\varphi \tag{16}$$

To obtain a closed system of equations for (F, G, ϕ), we divide Eqs. (14) and (15) by δ, and differentiate with respect to s:

$$(\cos\varphi)^{\cdot\cdot} = \left(\frac{F'}{\delta}\right)', \tag{17}$$

$$(\sin\varphi)^{\cdot\cdot} = \left(\frac{G'}{\delta}\right)', \tag{18}$$

$$\delta^2\ddot{\varphi} = (\delta^2\varphi')' + G\cos\varphi - F\sin\varphi. \tag{19}$$

3. Boundary conditions and conservation laws

The evolution of an initial impulse depends heavily on the boundary conditions. In this section we explain the various boundary conditions and their physical significance, and derive several conservation laws for the different cases.

The crack of the whip is created as the wave reaches the end of the whip and creates a rapid acceleration in the tip. The study of how this acceleration is produced will be done in two stages. First, we study the wave as it proceeds down the rod, when it is far from the end. By considering the wave to be travelling on an infinite rod, we can derive relations between the speed of the wave and the radius of the cross-section, and show that the speed of the wave increases as the rod tapers. Then, we turn our attention to the behavior of the rod as the wave reaches the end of the rod and the crack is produced. The study of the behavior of the wave as it reaches the end of the rod is performed numerically.

The first case we examine is a quasi-periodic, energy conserving case. In this case, the tension at the two ends of the rod is the same, and so does not represent the case of the whip, in which one end is free. However, by considering a loop travelling far from the end, and taking the ideal case in which the rod is infinite, we can make several deductions analytically. This case is also used as a benchmark for our numerical method as it has been studied extensively for the case of constant δ (for example [37,38]) and we extend some of these results to the case of a varying cross-sectional area.

For a real whip the end that cracks is *free*, that is, no force or moment is imposed. The boundary condition at this end is that the tension and curvature vanish. Thus, for the whip, the boundary condition at the free end is

$$\varphi' = F = G = 0. \tag{20}$$

We consider a whip of length L, where $s = 0$ corresponds to the point where the rod meets the handle of the whip and $s = L$ corresponds to the free end. There are several realistic conditions for the left (handle) end. We consider three cases, two in which the angle of the rod at the handle end is fixed, i.e. $\varphi(s = 0) = 0$, and one in which the rod at the handle end is allowed to swivel, i.e. $\varphi'(s = 0) = 0$. For the two cases in which the angle at the handle end is fixed, we consider one case in which a constant tension is applied at the handle end, and one in which the handle end is fixed. The latter case corresponds to the physical case of sending a loop down the rod, and then holding the handle end so that it does not move. The case of constant tension at the left end has the obvious physical significance of sending a loop down the rod and then pulling on the handle to give the tip a further kick. The four cases are considered as follows:

- Case I (quasi-periodic tension and angle):

$$\begin{aligned} &\varphi(b,t) = \varphi(a,t) + 2\pi k, \qquad \delta^2(a)\varphi'(a,t) = \delta^2(b)\varphi'(b,t), \qquad F(a,t) = F(b,t), \qquad G(a,t) = G(b,t),\\ &\delta(b)F'(a,t) = \delta(a)\,F'(b,t), \qquad \delta(b)G'(a,t) = \delta(a)G'(b,t). \end{aligned} \tag{21}$$

- Case II (no tension at right end, constant tension at left end):

$$\varphi'(b,t) = 0, \qquad F(b,t) = G(b,t) = 0, \qquad \varphi(a,t) = 0, \qquad F(a,t) = \alpha, \qquad G(a,t) = 0. \tag{22}$$

- Case III (no tension at right end, left end fixed):

$$\varphi'(b,t)=0, \qquad F(b,t)=G(b,t)=0, \qquad \varphi(a,t)=0, \qquad x(a,t)=y(a,t)=0. \tag{23}$$

- Case IV (no tension at right end, left end fixed, left end allowed to swivel):

$$\varphi'(b,t)=0, \qquad F(b,t)=G(b,t)=0, \qquad \varphi'(a,t)=0, \qquad x(a,t)=y(a,t)=0. \tag{24}$$

Of particular importance for our analysis is the role of conserved quantities such as energy and angular momentum. Systems (17)–(19) have several conservation laws (see [39]) of the form

$$T_t = X_s. \tag{25}$$

The first of these is related to the energy density

$$T = \tfrac{1}{2}[\delta^2\varphi_t^2 + \delta^2\varphi_s^2 + \delta(x_t^2 + y_t^2)], \tag{26}$$

$$X = \delta^2\varphi_s\varphi_t + Fx_t + Gy_t. \tag{27}$$

The *total energy* $\mathcal{H}$ is

$$\mathcal{H}(t) = \int_a^b T\,\mathrm{d}s = \frac{1}{2}\int_a^b [\delta^2\varphi_s^2 + \delta^2\varphi_t^2 + \delta(\dot{x}^2 + \dot{y}^2)]\,\mathrm{d}s, \tag{28}$$

where a and b are the endpoints of the rod, which may be infinite. The integrand of $\mathcal{H}$ can be written as the sum of a potential and a kinetic energy, $V + K$, where $V = \delta^2\varphi_s^2$, and $K = \delta^2\varphi_t^2 + \delta(\dot{x}^2 + \dot{y}^2)$. The potential energy $V = \delta^2\kappa^2$, which is the elastic energy of the rod. The first term of K is $\delta^2\dot{\varphi}^2 = \delta^2\omega^2$, which is the kinetic energy associated with a rotation of the basis vectors, or in other words, the rotational kinetic energy. The last term in K is δv^2, the translational kinetic energy. From the conservation law (25), we see that

$$\frac{\mathrm{d}}{\mathrm{d}t}\mathcal{H} = X(b,t) - X(a,t). \tag{29}$$

Thus, the energy at any given time depends on the boundary conditions. In Case I,

$$\frac{\mathrm{d}\mathcal{H}}{\mathrm{d}t} = F(b,t)\frac{\mathrm{d}}{\mathrm{d}t}\int_a^b \cos\varphi\,\mathrm{d}s + G(b,t)\frac{\mathrm{d}}{\mathrm{d}t}\int_a^b \sin\varphi\,\mathrm{d}s. \tag{30}$$

The boundary conditions (21) imply that

$$\frac{\mathrm{d}^2}{\mathrm{d}t^2}\int_a^b \cos\varphi\,\mathrm{d}s = \frac{\mathrm{d}^2}{\mathrm{d}t^2}\int_a^b \sin\varphi\,\mathrm{d}s = 0, \tag{31}$$

so that if

$$\frac{\mathrm{d}}{\mathrm{d}t}\left(\int_a^b \cos\varphi\,\mathrm{d}s\right)\bigg|_{t=0} = \frac{\mathrm{d}}{\mathrm{d}t}\left(\int_a^b \sin\varphi\,\mathrm{d}s\right)\bigg|_{t=0} = 0, \tag{32}$$

then energy is conserved,

$$\frac{\mathrm{d}\mathcal{H}}{\mathrm{d}t} = 0. \tag{33}$$

Eq. (32) is the compatibility conditions for conservation of energy in Case I, and we will assume that they hold throughout the paper when we discuss this case. In Case II, work is performed, so energy is not conserved, and

$$\mathcal{H} = -\alpha x(a,t) + \mathcal{H}(0). \tag{34}$$

In Cases III and IV, energy is conserved for all initial conditions satisfying the boundary conditions.

Another conservation law of the form (25) is given by

$$T = \delta^2\varphi_t + \delta x y_t - \delta y x_t, \tag{35}$$

$$X = \delta^2\varphi_s + Gx - Fy, \tag{36}$$

related to the *angular momentum* $\mathcal{L}$,

$$\mathcal{L}(t) = \int_a^b T = \int_a^b \delta^2\varphi_t + \delta x y_t - \delta y x_t \,\mathrm{d}s. \tag{37}$$

Angular momentum is only conserved in Case IV. We summarize the change in energy and angular momentum in the following table.

$$\begin{aligned}
&\text{Case I}: && \frac{\mathrm{d}}{\mathrm{d}t}\mathcal{H} = 0, && \frac{\mathrm{d}}{\mathrm{d}t}\mathcal{L} = G(a)\int_a^b \cos\varphi + F(a)\int_a^b \sin\varphi,\\
&\text{Case II}: && \frac{\mathrm{d}}{\mathrm{d}t}\mathcal{H} = -\alpha\dot{x}(a,t), && \frac{\mathrm{d}}{\mathrm{d}t}\mathcal{L} = -\delta^2(a)\varphi_s(a) + \alpha y(a),\\
&\text{Case III}: && \frac{\mathrm{d}}{\mathrm{d}t}\mathcal{H} = 0, && \frac{\mathrm{d}}{\mathrm{d}t}\mathcal{L} = -\delta^2(a)\varphi_s(a),\\
&\text{Case IV}: && \frac{\mathrm{d}}{\mathrm{d}t}\mathcal{H} = 0, && \frac{\mathrm{d}}{\mathrm{d}t}\mathcal{L} = 0.
\end{aligned} \tag{38}$$

Eqs. (14) and (15) are conservation laws themselves, associated with the *linear momenta* $\mathcal{M}^x$ and $\mathcal{M}^y$,

$$\mathcal{M}^x = \int_a^b \delta x_t \,\mathrm{d}s, \tag{39}$$

$$\mathcal{M}^y = \int_a^b \delta y_t \,\mathrm{d}s. \tag{40}$$

In Case I the linear momenta are conserved, but in Cases II–IV, they change in proportion to the tension at the left end.

4. Travelling wave solutions

The most efficient way to crack a whip is to send a planar loop down the whip (Fig. 4). Thus, a natural starting point for examining whip waves is the study of travelling wave solutions. The governing equations (17)–(19) support a travelling loop solution in the case of constant δ. If we consider a wave travelling far from the endpoints, it can be approximated by a wave travelling along an ideal infinite rod [40,41]. We will examine this case in order to determine how a wave is altered as the radius of the rod is decreased, but is still far away from the end of the rod. The boundary conditions consistent with the travelling loop solution are not consistent with the free end condition for the whip, so this analysis only provides us with some insights on how the speed changes when the loop is far from the end. We first consider the case where δ is constant, and look for travelling wave solutions of (17)–(19). Setting $\xi = s - ct$,

$$\delta c^2(\cos\varphi)'' = F'', \tag{41}$$

$$\delta c^2(\sin\varphi)'' = G'', \tag{42}$$

$$\delta^2(c^2-1)\varphi'' = G\cos\varphi - F\sin\varphi, \tag{43}$$

where $(\cdot)' = \mathrm{d}(\cdot)/\mathrm{d}\xi$. We consider an infinite rod which is horizontal at $-\infty$, and where the tension at $-\infty$ is α. This imposes the boundary conditions

$$\lim_{s\to-\infty}\varphi = \lim_{s\to-\infty} G = 0, \qquad \lim_{s\to-\infty} F = \alpha. \tag{44}$$

Integrating Eqs. (41) and (42) twice, and imposing the above boundary conditions, we find

$$F = \delta c^2\cos(\varphi) + \alpha - \delta c^2, \tag{45}$$

$$G = \delta c^2\sin(\varphi). \tag{46}$$

Substituting these into (43), we obtain the equation

$$\gamma^2\varphi'' = \sin(\varphi), \tag{47}$$

where

$$\gamma^2 = \frac{\delta^2(c^2-1)}{\delta c^2-\alpha}. \tag{48}$$

Eq. (47) is the "pendulum equation", with the well-known solution

$$\varphi = 4\tan^{-1}\left[\exp\left(\pm\frac{\xi-\xi_0}{\gamma}\right)\right]. \tag{49}$$

This solution corresponds to a loop travelling to the right with speed c. The $\pm$ sign in the exponent determines whether the loop is above or below the x-axis. We can find the space curve $\mathbf{R}$ by solving $x' = \cos(\varphi)$, $y' = \sin(\varphi)$, which yields (taking the $+$ sign, see Fig. 6)

$$x(s,t) = s - 2\gamma\tanh\left(\frac{s-ct}{\gamma}\right), \tag{50}$$

$$y(s,t) = 2\gamma\,\mathrm{sech}\left(\frac{s-ct}{\gamma}\right). \tag{51}$$

We see that Case I boundary conditions (21), and initial conditions (32) are satisfied, so the energy $\mathcal{H}$ is conserved. In fact, the energy on this solution is

$$\mathcal{H} = \frac{4\delta[2c^4\delta - \alpha(1+c^2)]}{\sqrt{(\delta c^2-\alpha)(c^2-1)}}. \tag{52}$$

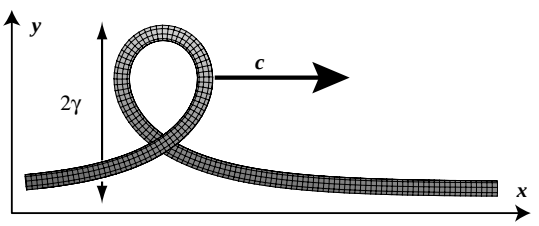

Fig. 6. Travelling wave solution.

We solve (48) for α, and using this in the above, we have two equations for δ and c:

$$\mathcal{H} = 4\delta\frac{\delta c^2 + \delta + \gamma^2 c^2}{\gamma}, \tag{53}$$

$$\alpha = \delta\frac{-\delta c^2 + \delta + \gamma^2 c^2}{\gamma^2}. \tag{54}$$

Therefore, we have a two-parameter family of travelling wave solutions depending on $(\mathcal{H}, \alpha)$, or alternatively, on (c, γ). We will see that (53) holds, to first order if δ is a slowly varying function of the arc-length s. Then, if the energy $\mathcal{H}$ is constant, we will have a way to solve for the speed c of the travelling wave as a function of δ, and hence of s, for a slowly varying radius of the cross-section.

We also note that the material point at the top of the loop travels at twice the speed of the loop itself. This is actually true for any travelling loop with constant shape and speed, regardless of the shape, by the following reasonings: (i) In the frame of reference moving at speed c, the speed of the travelling loop, all material points are travelling at the same speed c'. (ii) In the travelling frame of reference, the shape is constant, and the material points simply travel along the curve traced out by the loop. Therefore all points must travel at the same speed. (iii) The two speeds c' and c are equal. That is, in the travelling frame of reference, the speed of material points along the curve traced out by the loop is the same as the speed of the travelling loop. If we think of a point far to the right of the loop, then the loop is travelling toward this point with speed c in the fixed frame of reference. Therefore, in the moving frame of reference, this point is travelling toward the loop with speed c. So, when a material point reaches the top of the loop, it is travelling at speed c in the moving frame of reference travelling at speed c. When the point reaches the top of the loop, its velocity is tangential to the x-axis, so that it is travelling in the same direction as the loop itself. Thus, the velocity of the material point at the top of the loop is $2c$. This means that for a simple travelling wave, the maximal speed of a point on the rod is twice the speed of the travelling wave itself. Another way to look at the problem is to consider a vertical bicycle wheel rolled in a straight line at constant velocity c. A point on top of the wheel has a horizontal velocity c relative to the center of the wheel and hence an absolute horizontal velocity $2c$. This kinematic analysis of travelling waves on rods suggests a simple explanation of the observation by Krehl, Engemann and Schwenkel that the whip cracks when its maximal tip speed reaches about twice the speed of sound. We see that the loop reaches the speed of sound when the tip reaches twice the speed of sound. It suggests that it is the loop itself, and not the tip, that creates the shock which is not surprising since the loop is ahead of the tip and is subject to most of the interaction with the flow. However, this simple explanation will not suffice, due to the fact that the travelling wave solution does not satisfy the boundary conditions for the free end of a whip. When the travelling wave reaches the end of the whip it unfolds and the travelling loop shape is destroyed; a realistic analysis of the emission of the shock wave by a movable boundary accelerating in a supersonic flow is necessary to fully understand the nature of the phenomenon. Nevertheless, without a free boundary condition the maximal speed of a point on a rod with constant radius is twice the speed of the initial travelling loop.

5. Speed of travelling wave on a slowly varying background

Next we study how the travelling wave is affected by a change in the cross-sectional area. We start with the travelling wave solution (50) and (51) at $s = -\infty$, and let it travel in the positive s direction. How does the loop change as $\delta(s)$ changes? To conserve the energy, the speed may increase as the rod tapers or the speed could stay constant and the loop increase or decrease in size as to increase the kinetic or elastic energy. We show that for realistic initial conditions, the speed does increase and the loop size is essentially constant. We consider a rod whose cross-section is slowly varying, and expand the conservation law $T_t = X_s$ in ϵ. We show that, to first order, the

energy of the loop is constant. Doing so, one can write the speed of the travelling wave as a function of the slowly varying cross-sectional area.

Consider a rod whose radius $\delta = \delta(\epsilon s)$ varies slowly as a function of the arc-length, that is $\epsilon \ll 1$. We define the long space variable S, and the travelling wave variable ξ, as follows [22,42]:

$$S = \epsilon s, \tag{55}$$

$$\xi = \frac{1}{\epsilon}\int_0^S \zeta(\tilde{s})\,\mathrm{d}\tilde{s} - t. \tag{56}$$

Then,

$$\partial_t \to -\partial_\xi, \tag{57}$$

$$\partial_s \to \zeta(S)\partial_\xi + \epsilon\partial_S. \tag{58}$$

The motivation behind this change of variables is that we would like to determine how the speed and shape of the loop change when the cross-sectional area δ changes. For the travelling loop when δ is constant, $\zeta = 1/c$. We will see that, to first order, the speed of the loop is given by $1/\zeta(S)$, a function of the long space variable. The conservation law, in these variables, is

$$T_\xi + \zeta(S)X_\xi + \epsilon X_S = 0. \tag{59}$$

Expanding T, X and ζ in ϵ, and collecting terms in (59), we have

$$\mathcal{O}(\epsilon^0): \quad T_{0\xi} + \zeta_0 X_{0\xi} = 0, \tag{60}$$

$$\mathcal{O}(\epsilon^1): \quad T_{1\xi} + \zeta_1 X_{0\xi} + \zeta_0 X_{1\xi} + X_{0S} = 0. \tag{61}$$

Integrating the $\mathcal{O}(\epsilon^1)$ equation with respect to ξ, and assuming that T and X vanish at $\xi = \pm\infty$, we obtain the condition

$$\frac{\partial}{\partial S}\int_\infty^\infty X_0\,\mathrm{d}\xi = 0. \tag{62}$$

From the $\mathcal{O}(\epsilon^0)$ equation, we see that

$$\frac{\partial}{\partial S}\frac{1}{\zeta_0}\int_\infty^\infty T_0\,\mathrm{d}\xi = 0. \tag{63}$$

Note that (63) holds for an arbitrary conservation law $T_t = X_s$ with appropriate boundary conditions. Now we take T and X to be as in (26) and (27), and expand φ in ϵ, with φ_0 the travelling wave solution (49)

$$\varphi_0 = 4\tan^{-1}\left[\exp\left(\pm\frac{\xi}{\tilde{\gamma}}\right)\right]. \tag{64}$$

If we let

$$\tilde{\mathcal{H}} = \frac{1}{\zeta_0}\int_\infty^\infty T_0\,\mathrm{d}\xi, \tag{65}$$

then $\mathrm{d}\tilde{\mathcal{H}}/\mathrm{d}S = 0$. A straightforward calculation shows that

$$\tilde{\mathcal{H}} = \frac{4\tilde{\gamma}\delta}{\zeta_0}\left[\frac{\delta(1+\zeta_0^2)}{\tilde{\gamma}^2} + \frac{1}{\zeta_0^2}\right] + \mathrm{O}(\epsilon). \tag{66}$$

We see that the energy relation (53) holds, in the case when δ is a function of S, and that $\mathcal{H}$ is constant, to order ϵ.

The speed c and height 2γ of the loop, are given, to first order by

$$c(S) = \frac{1}{\zeta_0(S)}, \qquad \gamma(S) = \frac{\tilde{\gamma}}{\zeta_0(S)}. \tag{67}$$

We conclude that the relations (53) and (54) hold, in the case when δ is a function of S, and that $\mathcal{H}$ is constant, to order ϵ.

We can now use Eq. (53) to calculate the first order relation of the speed c as a function of δ. There are several cases, depending on the behavior of the tension and the height of the loop, α and γ. We will see in the numerical experiments below, with quasi-periodic boundary conditions on a finite interval, that the height of the loop remains mostly constant, while the tension at the ends varies.

Solving (53) for c, the speed of the loop is given by

$$c^2 = \frac{\gamma\mathcal{H}}{4\delta(\delta+\gamma^2)} - \frac{\delta}{\delta+\gamma^2}. \tag{68}$$

This equation gives the speed c of the loop as a function of δ, and hence of s, to first order, in the case when the height 2γ of the loop is constant, as in the quasi-periodic case. In the preceding equation $\mathcal{H}$ is determined by the speed of the loop at any given point, such as the initial condition. Then the relation gives the speed at each point along the rod. We see that the speed decreases as the rod tapers, as expected, and that $c \to \infty$ as the rod tapers to zero, $\delta \to 0$. Notice also that c as a function of δ passes through zero at $\delta = \sqrt{\gamma\mathcal{H}/4}$ and that there is no (real) solution for larger δ. Thus, a wave that is travelling on a rod whose cross-sectional area is *increasing* will slow down, and stop. At this reflection point all of the energy of the rod is potential. In the numerical experiments below, we show that the wave slows to zero speed, and then turns around and starts travelling in the opposite direction.

We may also consider the case of the infinite rod, in which the tension at the ends is held constant. In this case relations (53) and (54) hold, to first order, with α constant. We can thus calculate both the speed c and height 2γ as functions of the radius of the rod. A straightforward calculation shows that γ satisfies

$$f(\gamma) = \gamma^4 - \frac{\mathcal{H}}{4\alpha}\gamma^3 + \delta\gamma^2 + \frac{\mathcal{H}\delta}{4\alpha}\gamma - \frac{2\delta^3}{\alpha} = 0. \tag{69}$$

There are two cases, as illustrated in Fig. 7:

$$\text{Case 1}: \quad c \to \infty, \quad \gamma \to \frac{\mathcal{H}}{4\alpha} \quad \text{as } \delta \to 0, \tag{70}$$

$$\text{Case 2}: \quad c \to 1, \quad \gamma \to 0 \quad \text{as } \delta \to 0. \tag{71}$$

Note that the curves (δ, γ) and (δ, c) must pass through $(1, \cdot)$, since $\delta = 1$ is the reference cross-section, which is why in Fig. 7, only one branch of the curves represent the actual behavior of c and γ. Let δ^* be the point where two roots of $f(\gamma)$ become imaginary, and γ_l be the largest root of f. We see that in the case where $c \to 1$, $f'(\gamma_l)|_{\delta=\delta^*} = 0$, but in the case where $c \to \infty$, $f'(\gamma_l)|_{\delta=\delta^*} > 0$. Thus, a bifurcation occurs when $f'(\gamma_l)|_{\delta=\delta^*}$ goes to zero. Notice that at $\delta = \alpha$,

$$f(\gamma) = (\gamma^2 - \alpha)(4\alpha\gamma^2 - \mathcal{H}\gamma + 8\alpha^2). \tag{72}$$

Thus, at $\mathcal{H}^2 - 128\alpha^3 = 0$, two solutions coalesce. This is, in fact, the bifurcation point, because, at this point, $\gamma_l = \gamma^* = \mathcal{H}/8\alpha = \sqrt{2}\alpha^{-3/2}$,

$$f(\gamma^*)|_{\mathcal{H}^2=128\alpha^3} = f'(\gamma^*)|_{\mathcal{H}^2=128\alpha^3} = 0, \tag{73}$$

$$f''(\gamma^*)|_{\mathcal{H}^2=128\alpha^3} = 2\alpha > 0, \tag{74}$$

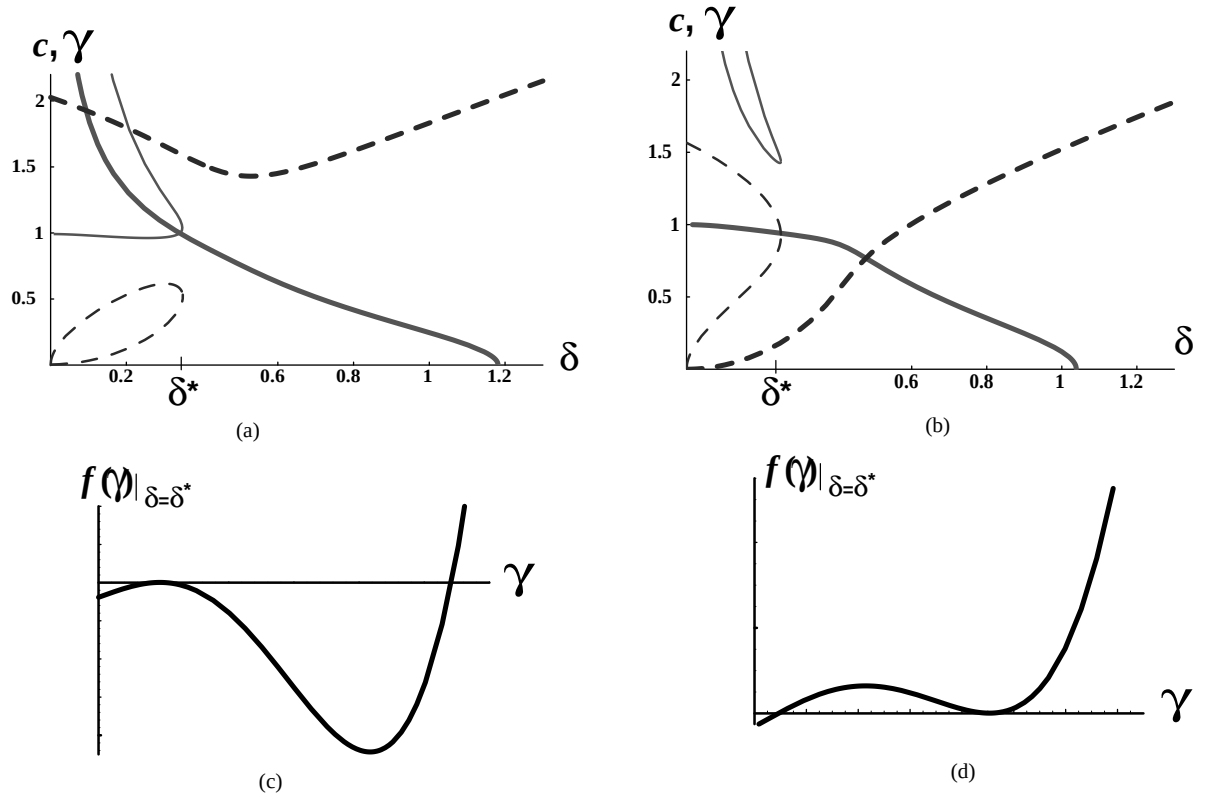

Fig. 7. Two possibilities: either (a) c goes to ∞, or (b) c goes to 1 as $\delta \to 0$. The solid curve is c; the dash-dotted curve is γ. The thicker curves are the curves representing the behavior of c and γ. The graphs (c) and (d) represent $f(\gamma)$ in the cases (a) and (b), respectively, at $\delta = \delta^*$, where δ^* is the point where two roots of $f(\gamma)$ become imaginary.

and the γ and c curves cross at

$$\delta = \alpha, \quad \gamma = \sqrt{2}\alpha^{-3/2}, \qquad \delta = \alpha, \quad c = 1, \tag{75}$$

respectively. The behavior of c as $\delta \to 0$ also depends on which branch of the curve c is on. Since γ and c must be defined at $\delta = 1$, the reference ratio of areas, we define the *initial* speed and height of the travelling wave to be at $\delta = 1$:

$$c_\mathrm{i} = c(\delta = 1), \qquad \gamma_\mathrm{i} = \gamma(\delta = 1). \tag{76}$$

We note that if $c_\mathrm{i} > 1$ then $c \to \infty$ as $\delta \to 0$. Therefore, we have the conditions

$$\text{if } \ \mathcal{H}^2 - 128\alpha^3 > 0 \quad \text{or} \quad c_\mathrm{i} > 1 \quad \text{then } \ c \to \infty, \ \ \gamma \to \tfrac{1}{4}(\mathcal{H})\alpha \ \text{ as } \ \delta \to 0, \tag{77}$$

$$\text{if } \ \mathcal{H}^2 - 128\alpha^3 < 0 \quad \text{and} \quad c_\mathrm{i} < 1 \quad \text{then } \ c \to 1, \ \ \gamma \to 0 \ \text{ as } \ \delta \to 0. \tag{78}$$

Since the radius of the rod in the scaled variables is 2, it must be that $\gamma_\mathrm{i} > 2$ to be physically realistic. We compute the behavior for realistic rods as follows. Note that

$$\mathcal{H}^2 - 128\alpha^3 = \frac{16}{\gamma i^6}\{\gamma_\mathrm{i}^4[1 + c_\mathrm{i}^2(\gamma_\mathrm{i}^2 + 1)]^2 - 8[1 + c_\mathrm{i}^2(\gamma_\mathrm{i}^2 - 1)]^3\}. \tag{79}$$

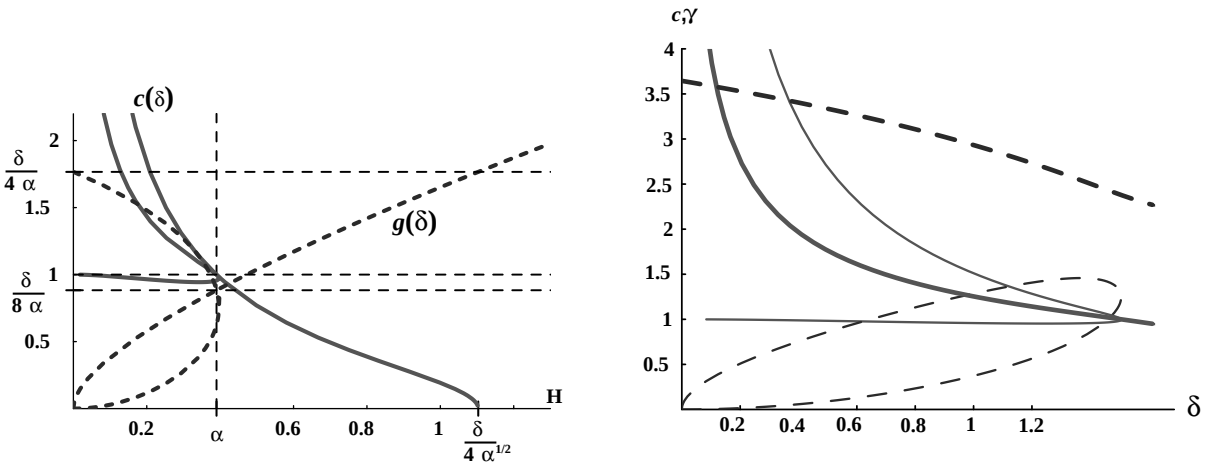

(a) (b)

Fig. 8. (a) The curves c and γ at the bifurcation point, $\mathcal{H}^2 - 128\alpha^3 = 0$. (b) If $c_\mathrm{i} > 1$ then $c \to \infty$ as $\delta \to 0$.

Thus, for $0 \le c_\mathrm{i} \le 1$, $\gamma_\mathrm{i} \ge 1$,

$$\begin{aligned}\mathcal{H}^2 - 128\alpha^3 &\ge \frac{16}{\gamma_\mathrm{i}^6}\{\gamma_\mathrm{i}^4[1 + c_\mathrm{i}^2(\gamma_\mathrm{i}^2 - 1)]^2 - 8[1 + c_\mathrm{i}^2(\gamma_\mathrm{i}^2 - 1)]^3\} \\ &= \frac{16}{\gamma_\mathrm{i}^6}[1 + c_\mathrm{i}^2(\gamma_\mathrm{i}^2 - 1)]^2\{\gamma_\mathrm{i}^4 - 8[1 + c_\mathrm{i}^2(\gamma_\mathrm{i}^2 - 1)]\} > 0 \end{aligned} \tag{80}$$

if $\gamma_\mathrm{i} > 2^{3/4}$. Since we assume that the initial speed of a loop is subsonic, and the radius of the rod is 2, all physically realistic solutions have $0 \le c_\mathrm{i} \le 1$, $\gamma_\mathrm{i} \ge 2^{3/4}$. Thus, for all physically realistic cases $c \to \infty$ as $\delta \to 0$.

We further note that, as in the case of constant loop size, in the case when the tension is held constant, a loop travelling on a rod whose cross-sectional area is *increasing* will slow down, and stop. The point at which the wave stops is determined by finding the value of $\delta = \mathcal{H}/4\sqrt{\alpha}$ such that $c = 0$ (see Figs. 7 and 8).

6. Numerical simulations

We now turn to a complete description of the behavior of the whip with realistic boundary conditions. The analysis presented above can only be applied away from the end when the assumptions on the variation of tension and the boundary conditions are valid. Close to the end, a numerical analysis is necessary to complete the description. A dedicated scheme for solving (17)–(19) was developed by Falk and Xu [38,43,44]. This scheme was developed for the particular case (Case I) of a constant radius and periodic boundary conditions. We present an extension of the scheme to incorporate the varying radius and different boundary conditions. While the inclusion of tapering in the algorithm is straightforward the main challenge is to adapt it as to include different types of realistic boundary conditions and prove the conservation of discrete versions of the conservation laws (such as energy and angular momentum).

We discretize the interval $[0, L]$ into N equally spaced mesh points s_j, $s_{j+1} - s_j = L/N = h$, and time is discretized into steps of duration τ, with the ratio $\nu = \tau/h$ set equal to 1/2, below the limit of the classical CFL

condition for stability, $\nu = 1/\sqrt{2}$ (cf. [45, p. 489]). The discrete version of (17)–(19) is

$$\Delta_\tau^2 \cos\theta_j^n = \Delta_h^+ \left\{ \frac{1}{\delta_j} \Delta_h^- f_j^n \right\}, \tag{81}$$

$$\Delta_\tau^2 \sin\theta_j^n = \Delta_h^+ \left\{ \frac{1}{\delta_j} \Delta_h^- g_j^n \right\}, \tag{82}$$

$$\Delta_\tau^2 \theta_j^n - \Delta_h^2 \theta_j^n = \frac{1}{\delta_j^2} \Delta_h^+ \delta_j^2 \Delta_h^+ \theta_j^n + \frac{1}{\delta_j^2} [g_j^n C^n(\theta_j) - f_j^n S^n(\theta_j)], \tag{83}$$

where

$$S^n(\theta_j) = \begin{cases} \dfrac{-(\cos\theta_j^{n+1} - \cos\theta_j^{n-1})}{\theta_j^{n+1} - \theta_j^{n-1}} & \text{if } \theta_j^{n+1} \neq \theta_j^{n-1}, \\ \sin\theta_j^{n-1} & \text{if } \theta_j^{n+1} = \theta_j^{n-1}, \end{cases} \tag{84}$$

$$C^n(\theta_j) = \begin{cases} \dfrac{\sin\theta_j^{n+1} - \sin\theta_j^{n-1}}{\theta_j^{n+1} - \theta_j^{n-1}} & \text{if } \theta_j^{n+1} \neq \theta_j^{n-1}, \\ \cos\theta_j^{n-1} & \text{if } \theta_j^{n+1} = \theta_j^{n-1}, \end{cases} \tag{85}$$

$\delta_j = \delta(hj)$, and θ_j^n, f_j^n, and g_j^n are approximate values of $\varphi(jh, n\tau)$, $F(jh, n\tau)$, and $G(jh, n\tau)$. The discrete derivatives are defined by

$$\Delta_\tau^2 u_j^n = \frac{1}{\tau^2}(u_j^{n+1} - 2u_j^n + u_j^{n-1}), \qquad \Delta_h^2 u_j^n = \frac{1}{h^2}(u_{j+1}^n - 2u_j^n + u_{j-1}^n), \tag{86}$$

$$\Delta_h^- u_j^n = \frac{1}{h}(u_j^n - u_{j-1}^n), \qquad \Delta_h^+ u_j^n = \frac{1}{h}(u_{j+1}^n - u_j^n). \tag{87}$$

The discrete versions of x and y are,

$$x_j^n = x_a^n + h \sum_{i=1}^{j-1} \cos\theta_i^n, \tag{88}$$

$$y_j^n = y_a^n + h \sum_{i=1}^{j-1} \sin\theta_i^n, \tag{89}$$

where x_a^n and y_a^n will be determined from the conditions

$$\Delta_\tau^2 x_j^n = \frac{1}{\delta_j} \Delta_h^- f_j^n, \tag{90}$$

$$\Delta_\tau^2 y_j^n = \frac{1}{\delta_j} \Delta_h^- g_j^n. \tag{91}$$

It is clear from the definition that

$$\Delta_h^+ x_j^n = \cos\theta_j^n, \tag{92}$$

$$\Delta_h^+ y_j^n = \sin\theta_j^n. \tag{93}$$

The discrete boundary conditions, corresponding to the four cases (21)–(24), are:

- Case I (quasi-periodic tension and angle):

$$f_0^n = f_N^n, \qquad g_0^n = g_N^n, \qquad \theta_0^n + 2\pi k = \theta_N^n, \qquad \delta_0^2(\theta_1^n - \theta_0^n) = \delta_N^2(\theta_{N+1}^n - \theta_N^n),$$
$$\delta_1(f_{N+1}^n - f_N^n) = \delta_{N+1}(f_1^n - f_0^n), \qquad \delta_1(g_{N+1}^n - g_N^n) = \delta_{N+1}(g_1^n - g_0^n). \tag{94}$$

- Case II (no tension at right end, constant tension at left end):

$$f_0^n = \alpha, \qquad g_0^n = 0, \qquad g_N^n = f_N^n = 0, \qquad \theta_{N+1}^n = \theta_N^n, \qquad \theta_0^n = 0. \tag{95}$$

- Case III (no tension at right end, left end fixed):

$$f_N^n = g_N^n = 0, \qquad \theta_{N+1}^n = \theta_N^n, \qquad \theta_0^n = 0, \qquad x_a^n = y_a^n = 0. \tag{96}$$

- Case IV (no tension at right end, left end fixed, left end allowed to swivel):

$$f_N^n = g_N^n = 0, \qquad \theta_{N+1}^n = \theta_N^n, \qquad \theta_0^n = \theta_1^n, \qquad x_a^n = y_a^n = 0. \tag{97}$$

The main idea behind the scheme is to solve (81) and (82) for f_j^n, g_j^n, and use these values to form one semilinear equation for θ_j^n from (83), which is solved for θ_j^{n+1}, iteratively. The method is designed to preserve a discrete version of the energy. The discrete energy is given by

$$E_n = \frac{h}{2}\sum_{j=1}^{N}\{\delta_j^2(\Delta_\tau^+\theta_j^n)^2 + \delta_j^2(\Delta_h^-\theta_j^n)(\Delta_h^-\theta_j^{n+1}) + \delta_j[(\Delta_\tau^+x_j^n)^2 + (\Delta_\tau^+y_j^n)^2]\}. \tag{98}$$

Conservation of energy is central to the development of the method, so we first present the following lemma (for a proof see Appendix A).

Lemma 6.1. *For every $n \geq 0$, we have $E_{n+1} = E_n + R_n$, where R_n is given by*

$$R_n = \tfrac{1}{2}[\delta_{N+1}^2\Delta_h^+\theta_N^n(\theta_N^{n+1} - \theta_N^{n-1}) - \delta_1^2\Delta_h^+\theta_0^n(\theta_0^{n+1} - \theta_0^{n-1}) + f_N^n(x_{N+1}^{n+1} - x_{N+1}^{n-1})$$
$$- f_0^n(x_1^{n+1} - x_1^{n-1}) + g_N^n(y_{N+1}^{n+1} - y_{N+1}^{n-1}) - g_0^n(y_1^{n+1} - y_1^{n-1})]. \tag{99}$$

We see how the energy is conserved in the four cases. In Case I, the equations and boundary conditions imply that

$$\Delta_\tau^2\sum_{j=1}^{N}\cos\theta_j^n = 0. \tag{100}$$

Thus, if

$$\sum_{j=1}^{N}\cos\theta_j^0 = \sum_{j=1}^{N}\cos\theta_j^1, \tag{101}$$

$$\sum_{j=1}^{N}\sin\theta_j^0 = \sum_{j=1}^{N}\sin\theta_j^1, \tag{102}$$

then $R_n = 0$, and the discrete energy is conserved in Case I. In [43], Coleman and Xu present an algorithm for calculating $\theta_j^{0,1}$ such that (101) and (102) hold.

In Case II, we have

$$R_n = -\tfrac{1}{2}(\alpha)(x_1^{n+1} - x_1^{n-1}). \tag{103}$$

In Cases III and IV, $R_n = 0$, and the discrete energy is conserved. We also define the discrete angular momentum

$$L_n = h\sum_{j=1}^{N}\{\delta_j^2\Delta_\tau^+\theta_j^n + \delta_j(x_j^n\Delta_\tau^+ x_j^{n-1} - y_j^n\Delta_\tau^+ y_j^{n-1})\}. \tag{104}$$

The discrete angular momentum is not conserved in any of the four cases. This is due to the fact that we use an approximation for the cosine and sine in (83), but fluctuations in the discrete angular momentum in Case IV are very small, and decrease to zero as the number of spatial points is increased. Details on the numerical scheme and its implementation are provided in Appendix A.

6.1. Numerical results

As a benchmark, we first compare the results in the quasi-periodic case, starting with the known travelling wave solution, to see that the analytic solution is recovered. We also verify that the energy is conserved, and matches the analytically determined energy. Fluctuations in the energy occur because of the necessity of accepting an approximate solution to the semi-linear equation (A.30) for θ_j^n, and in Case I additional fluctuations occur due to the fact that $\sum \cos\theta_j^n$ is not conserved exactly. In Case I, fluctuations in the energy were always less than 0.008%, and in Cases III and IV always less than 0.00005%. In Case IV, where the analytical angular momentum is conserved, the fluctuations in the discrete angular momentum were always less than 0.0007%.

Case I. Results of numerical calculations for constant δ are summarized by Coleman and Xu [43]. When we allow the radius of the rod to vary, we obtain results consistent with the analytical predictions, i.e. that the speed increases or decreases as the cross-sectional area decreases or increases, according to relation (68) the speed of the loop is given by

$$c^2 = \frac{\gamma\mathcal{H}}{4\delta(\delta+\gamma^2)} - \frac{\delta}{\delta+\gamma^2}. \tag{105}$$

Calculations in Case I are done in the scaled variables. Figs. 9 and 10 show results in the case where the radius is decreasing, and Figs. 9 and 10 show results in the case where the radius is increasing. From Figs. 9 and 11 we see that the height of the loop remains almost constant as the speed increases and decreases, respectively. This is, in fact, generally true. Thus, we may calculate the speed of the travelling loop from (105) and compare it with the speed calculated numerically. In Figs. 10B and 12B we see that the analytically and numerically computed speeds match almost identically. In Figs. 10 and 12 are two graphs. In graph (A) we show the speed of the loop as a function of time. On the same graph is shown the value of δ at the material point at the top of the loop. In graph (B) the speed of

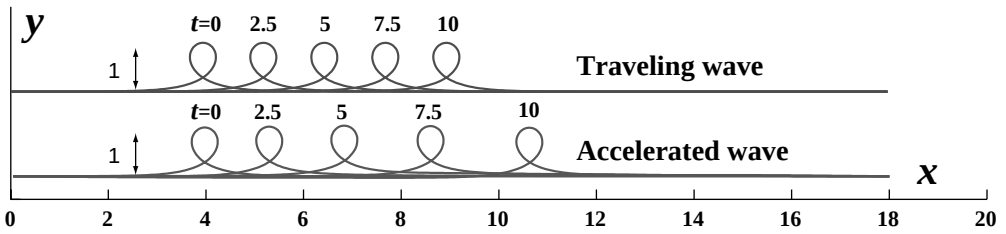

Fig. 9. Traveling wave solution with $\delta = 1$ (top) and numerical solution at times $t = 0, 2.5, 5, 7.5, 10$ with $\delta(s) = 1 - (1/2)(s/L)$.

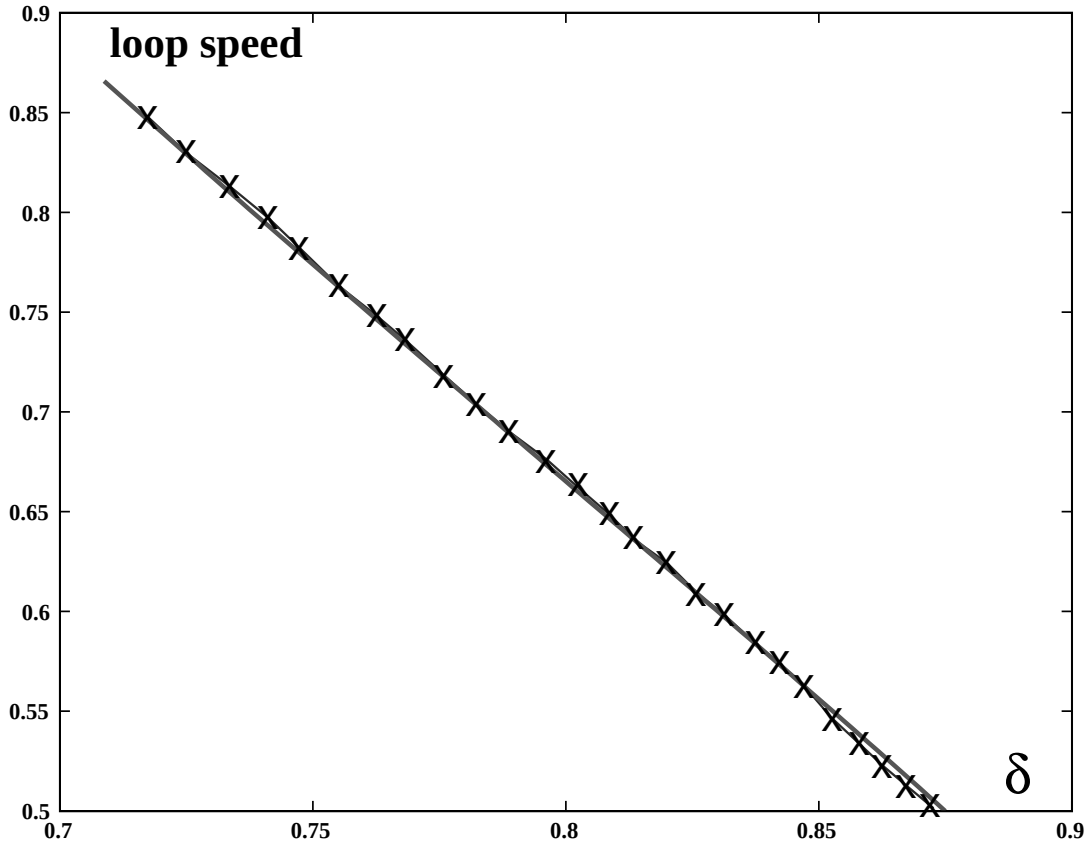

Fig. 10. Speed of loop as a function of δ with $\lambda = 1/2$. The solid curve is the analytically computed speed of the loop, as determined from (105), and the +'s are the numerically computed speed of the loop.

the loop is shown as a function of δ, by computing the speed of the loop at each time step, and plotting that against the value of δ at the material point at the top of the loop. In Figs. 11 and 12 are shown the results of calculations for a rod whose radius is increasing. We see that the speed of the loop decreases to zero, and then the loop turns around and travels in the opposite direction.

Case II. In order to measure the effects of the boundary conditions, tension and tapering in the rod on the maximal speed of the tip of the rod, we must take into account how the material points behave without these effects. Since the speed of the material point at the top of a travelling loop is twice the speed of the loop itself, we define a new quantity to measure the increase of the maximum speed of a material point on the rod:

$$\sigma = \frac{\text{maximum speed of tip}}{2c_{\mathrm{i}}}, \tag{106}$$

where c_{i} is the initial speed of the loop. We see that without the free boundary condition, and without tapering, for the travelling loop, $\sigma = 1$. Thus, σ measures the increase in the maximal speed of the tip due to the various effects we consider. For the simulations in which we compare the tapering and the tension to the maximum speed of the tip, we take the initial loop to be centered on the rod, that is, the top of the loop is at $s = L/2$. The tapering of the rod is chosen to be a linear function,

$$\delta(s) = 1 - \lambda\frac{s}{L}. \tag{107}$$

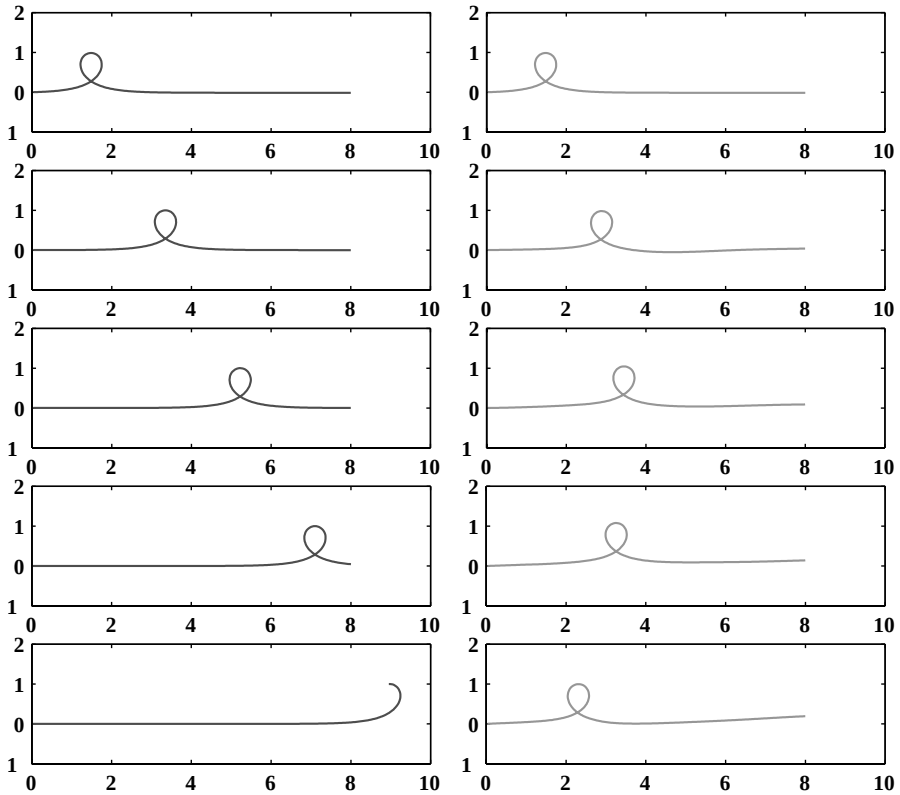

Fig. 11. Traveling wave for $\delta = 1$ (left) and numerical solution at times $t = 0, 3.75, 7.5, 11.25, 15$ with $\delta(s) = (1/2)(1 + (s/L))$.

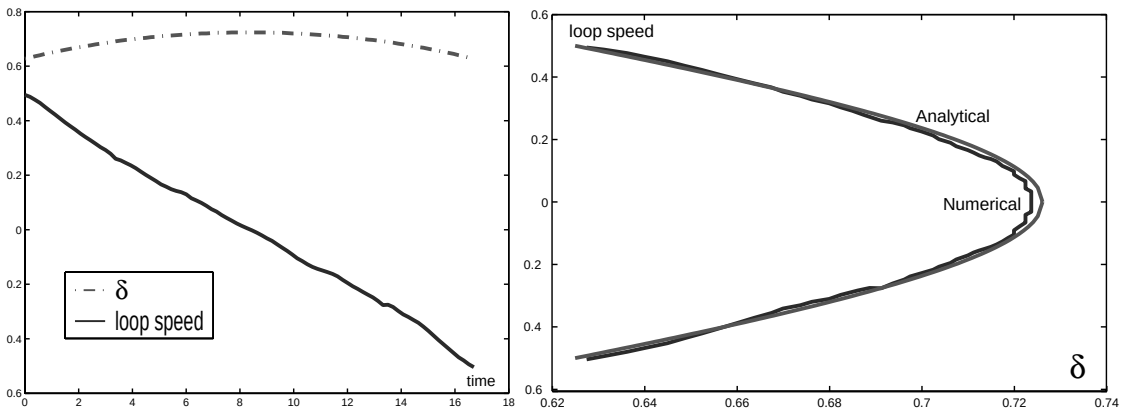

(A) (B)

Fig. 12. (A) Speed of loop and δ at the top of the loop as a function of time, for an increasing radius, $\delta(s) = (1/2)(1 + (s/L))$. (B) Speed of loop as a function of δ. The analytical curve is computed from (105).

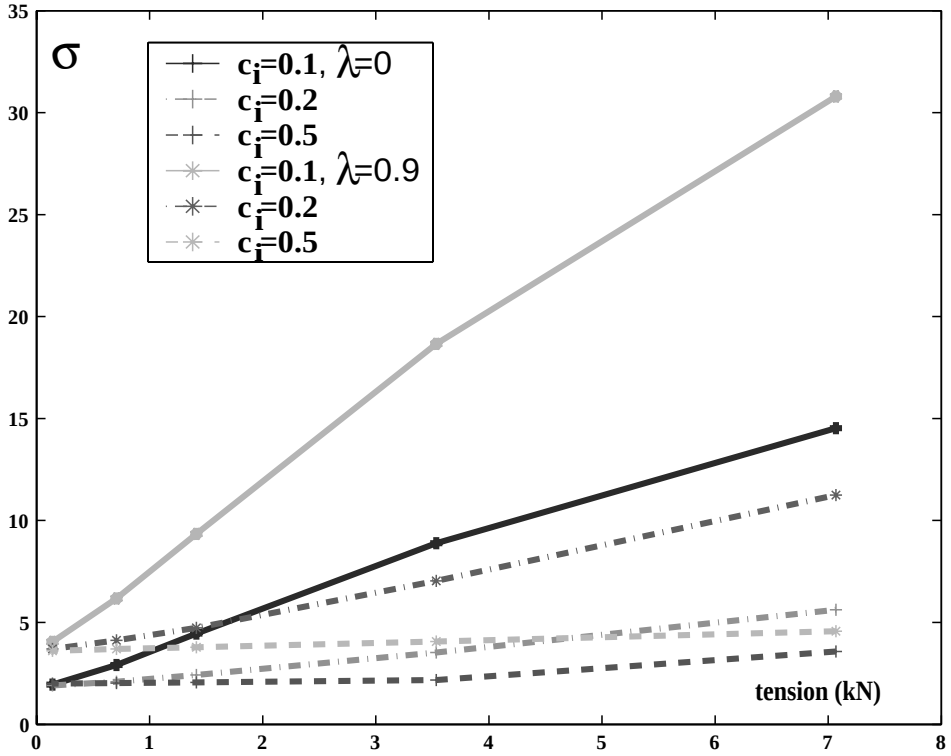

Fig. 13. Maximum tip speed vs. tension at handle in Case II. In this case, the rod is 2 m long, and the typical radius is 1 cm. The height of the initial loop $2\gamma_1$ is $\gamma_1 = L/10$.

Thus, λ is a measure of the tapering in the rod. A rod without tapering has $\lambda = 0$, and a rod that tapers to zero radius at its tip has $\lambda = 1$.

When we apply a fixed tension at the handle end, energy is not conserved, as work is performed when the left end accelerates. In Fig. 13 we see that the maximum tip speed increases (almost) linearly as the tension applied at the left end increases. No general relation between σ and the tension applied at the handle is computed, as the maximal tip speed depends also on the initial speed and size of the loop. However, we see that for a given initial speed and size of the loop, the maximal tip speed is almost linear in the applied tension. We also note that the acceleration of the tip is greater when the initial speed of the loop is smaller, although the final tip speed is greater for a faster initial speed. In Fig. 14 we see the result of one simulation in Case II, as the whip unfolds. In this case, the loop is started toward the right end of the rod, and a large tension is applied at the left end. If one applies the same tension with a loop at the middle of the rod, the loop is simply pulled through, and the acceleration of the tip is not great. Such a case is seen in Fig. 15. The lesson is that in order to produce a large acceleration in the tip, the loop must accelerate until it is close to the end of the rod. This is consistent with the way whips are cracked: one sends a loop down the rod, which accelerates as the rod tapers, and then one applies a tension as the loop reaches the end of the rod to provide an extra kick. In this way, a large acceleration, with an associated loud crack, is produced.

Case III. In Fig. 16 we see the results of several simulations, in which the maximum speed of the tip is compared with the tapering in the rod. We show several simulations with different values of the tapering λ. We see that for an untapered rod, for which $\lambda = 0$, the maximum speed of the tip is between 4 and 6 times the initial speed of the loop,

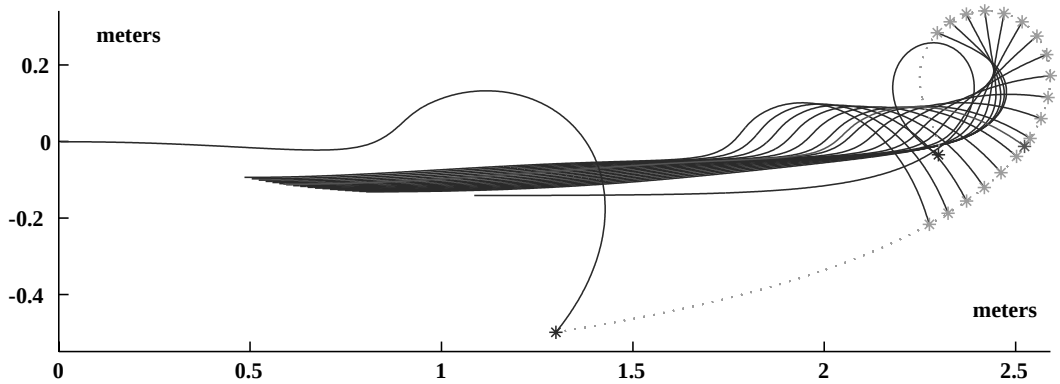

Fig. 14. Unfolding of tip in Case II. The rod is 2 m long, and the typical radius is 1 cm; initial speed and height of loop are $c_i = 0.5$, $\gamma_i = L/10$; applied tension is 120 kN. Elapsed time is 0.007 s.

or σ is between 2 and 3, the acceleration due solely to the free boundary condition. This acceleration, sometimes refer to as the "Kucharski effect" is due to the rotation of the tip around the horizontal axis as the loop reaches the end [16]. As the tapering increases the maximum speed of the tip increases. At the maximal tapering, when the area of the cross-section at the end of the tip is 1/20 the area at the handle, we get another doubling of the maximum tip speed. Again, no general relation between the tapering and the maximal tip speed has been found analytically, but a general trend can be observed. The maximal tip speed increases nonlinearly as a function of the tapering, with no obvious scaling. We do see, however, that the tapering has a greater effect on the maximal tip speed than does the increase of applied tension in Case II. As in Case II, acceleration is greater for a slower initial speed, although for a greater initial speed, the maximal tip speed is greater. Fig. 17 shows a result of one simulation in this case, as the tip of the whip unfolds.

Case IV. Results in Case IV, where the whip is allowed to swivel at the handle, are essentially indistinguishable from Case III. That is, there seems to be no advantage or disadvantage in allowing the swiveling, at least in the case where a loop is sent down the whip as we have prescribed. This could explain why there seems to be no preference among whip-makers for swiveling or non-swiveling thongs.

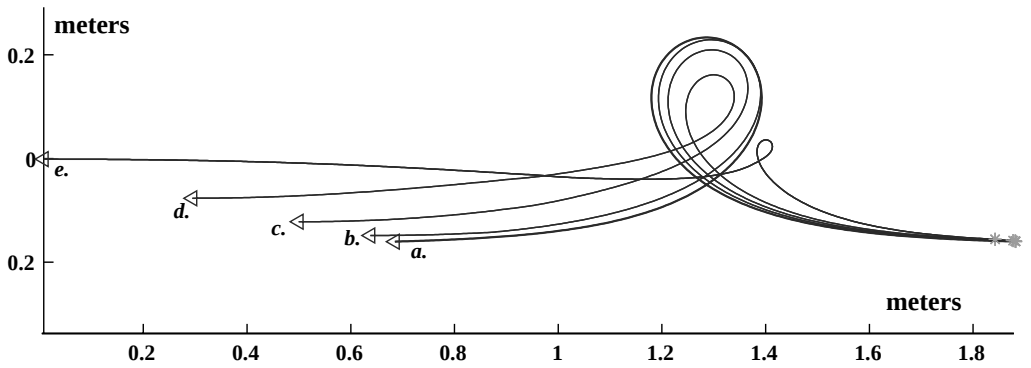

Fig. 15. High tension applied too early in Case II. The rod is 2 m long, and the typical radius is 1 cm; initial speed and height of loop are $c_i = 0.1$, $\gamma_i = L/10$; applied tension is 80 kN. The triangles are the left (handle) end of the whip, and the thicker curve is the initial condition. Elapsed time is 0.005 s.

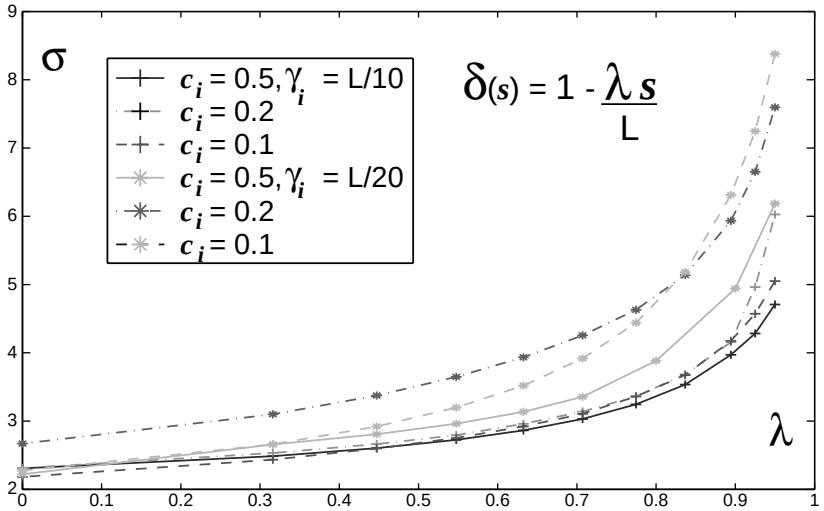

Fig. 16. Maximum tip speed vs. tapering of cross-sectional area in Case III. In this case, the rod is 2 m long, and the typical radius is 1 cm.

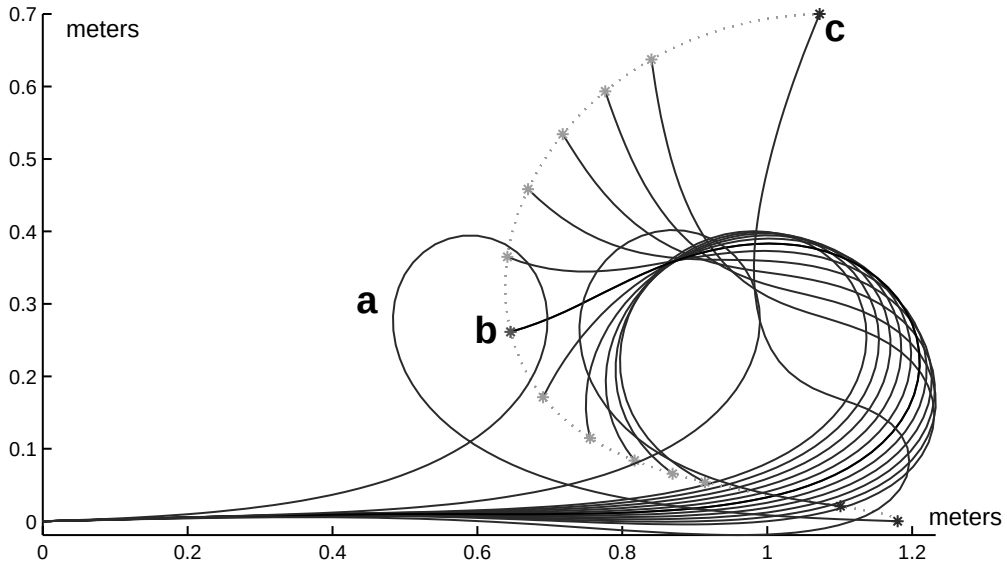

Fig. 17. Unfolding of tip in Case III. The rod is 2 m long, and the typical radius is 1 cm; initial speed and height of loop are $c_1 = 0.5$, $\gamma_1 = L/10$. There is no tapering. Curve (a) is the initial condition, curve (b) is the rod at the time of the maximal speed of the tip, and curve (c) is the rod at the end time, 0.02 s.

7. Shock waves

A whip produces a crack when a section of the whip travels faster than the speed of sound and creates a mini sonic boom. We have already addressed the puzzling observation of Krehl et al. concerning the speed of the tip as the shock wave is emitted. The main question is which part of the whip is actually creating the sonic boom, the

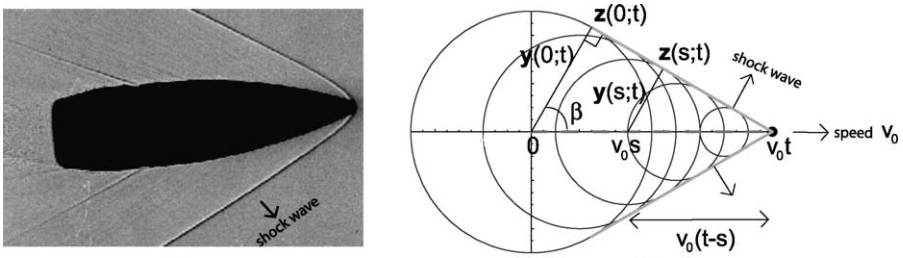

(a) (b)

Fig. 18. The Mach cone of an object travelling in a straight line. (b) A bullet travelling faster than the speed of sound. (b) Illustration of the Mach cone. The thinner circles are the sound waves, the thicker lines are the shock waves. The dashed line is the path of the object.

tip or a section of the whip. To try to answer this question, we compute the geometric (linear) shock wave that is emitted by the tip as the whip unfolds.

When an object travels faster than the speed of sound, a *shock wave* is formed. For an object travelling in a straight line, the first approximation of the shock wave is given by the *Mach cone*, because the shock wave is in the shape of a cone following the object. This phenomenon can be observed, for example, in the wake that follows a swiftly moving boat, or in the shock wave following a bullet, as in Fig. 18a. We now compute a similar approximation for the shape of the shock wave in the case of an object travelling in an arbitrary path. We will apply this to the case of the tip of the cracking whip to see how the shock wave emanates from a cracking whip.

In the linear theory, a shock wave is formed by the envelope of infinitely many sound wave fronts meeting at the same curve. Consider first the case of an object travelling with constant speed along a straight line, as in Fig. 18. Let the speed of sound be v_s, and the speed of the object be v_0. If the object leaves the origin at time 0, it reaches $(v_0 t, 0)$ at time t. Thus, let $\mathbf{x}(s) = (v_0 s, 0)$ be the path of the object. At each point s the object emits a sound wave, whose front at time t is a circle centered at $(v_0 s, 0)$, with radius $v_s(t - s)$. The shock wave is the envelope of these sound waves. At time t this is a curve which we call $\mathbf{z}(s; t)$.

We calculate the shock wave curve $\mathbf{z}(s; t)$ as follows. Let $\mathbf{y}(s; t)$ be the line from $(v_0 s, 0)$ to the tangent of the circle to $\mathbf{x}(t) = (v_0 t, 0)$. The Mach cone $\mathbf{z}$ is then determined as the set of all the tangent points. The angle between $\mathbf{y}(s; t)$ and $\mathbf{x}(s; t)$ is determined by the condition

$$\cos\beta = \frac{|\mathbf{y}(s;t)|}{v_0(t-s)} = \frac{v_s(t-s)}{v_0(t-s)} = \frac{v_s}{v_0}. \tag{108}$$

Thus, the envelope $\mathbf{z}(s; t)$ is given by

$$\mathbf{z}(s;t) = (v_0 s, 0) + \mathbf{y}(s;t), \tag{109}$$

where $\mathbf{y}(s; t)$ is determined by the system

$$(1,0)\cdot\frac{\mathbf{y}(s;t)}{|\mathbf{y}(s;t)|} = \frac{v_s}{v_0}, \tag{110}$$

$$|\mathbf{y}(s;t)| = v_s(t-s). \tag{111}$$

The envelope $\mathbf{z}(s; t)$ is a space curve defined for every $t > 0$, for $0 \le s \le t$. In this case of an object travelling on a straight path with constant velocity, as in Fig. 18, the Mach cone at each time t, is given by

$$\mathbf{z}(s;t) = \left(s + \frac{1}{v_0^2}(t-s), \pm(t-s)\sqrt{\frac{1}{v_0^2-1}}\right). \tag{112}$$

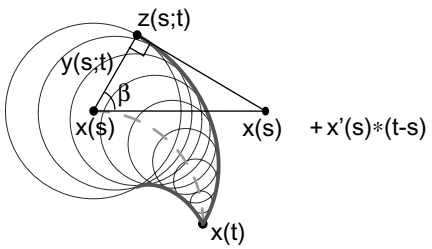

Fig. 19. The shock wave of an object travelling in a curved path. The thinner circles are the sound waves, the thicker lines are the shock waves. The dashed line is the path of the object.

The case of an object travelling on a straight path can be easily generalized to the case of an object travelling along an arbitrary path, $\mathbf{x}(s)$. Again, the envelope of the sound waves, which is the shock wave, is given by the curve $\mathbf{z}(s;t)$. Apparently (see Fig. 19), $\mathbf{z}$ is given by

$$\mathbf{z}(s;t) = \mathbf{x}(s) + \mathbf{y}(s;t), \tag{113}$$

where $\mathbf{y}(s;t)$ is determined by the system

$$\frac{\mathbf{x}'(s)}{|\mathbf{x}'(s)|} \cdot \frac{\mathbf{y}(s;t)}{|\mathbf{y}(s;t)|} = \frac{v_s}{v_0}, \tag{114}$$

$$|\mathbf{y}(s;t)| = v_s(t-s). \tag{115}$$

We can further generalize the above to the case of an object travelling along an arbitrary path with an arbitrary speed. In the above, we have assumed that the speed of the object v_0 is constant, or in other words that $|\mathbf{x}'(s)| \equiv v_0 = \text{constant}$. Now we allow that $\mathbf{v}(s) = \mathbf{x}'(s)$ varies along the path of the object. The distance the object travels from s to t is

$$\mathrm{d}(s;t) = \int_s^t |\mathbf{v}(s')|\,\mathrm{d}s'. \tag{116}$$

Then, the shock wave is still given by (113), but with $\mathbf{y}$ defined by

$$\frac{\mathbf{x}'(s)}{|\mathbf{x}'(s)|} \cdot \frac{\mathbf{y}(s;t)}{|\mathbf{y}(s;t)|} = \frac{v_s(t-s)}{\int_s^t |\mathbf{v}(s')|\,\mathrm{d}s'}, \tag{117}$$

$$|\mathbf{y}(s;t)| = v_s(t-s). \tag{118}$$

We note, also, that the above formulation is valid in three dimensions as well. Given a path $\mathbf{x}(s)$, in three-space, the shock wave is defined by (113), where $\mathbf{y}$ is defined by (117) and (118). The difference now is that these equations define a curve, instead of two points, for each s, t. The shock wave, for each time t, is then a surface in three-space. For example, an object travelling at constant speed v_0 along the x-axis would have the Mach cone,

$$\mathbf{z}(s,\theta;t) = \left(s + \frac{1}{v_0^2}(t-s),\ \cos(\theta)(t-s)\sqrt{\frac{1}{v_0^2-1}},\ \sin(\theta)(t-s)\sqrt{\frac{1}{v_0^2-1}}\right), \tag{119}$$

a surface for each time t.

7.1. Numerical computation of shock waves

We now compute the shock wave which is the crack of the whip, for the simulation seen in Fig. 14. In Fig. 20 we see the results of this calculation, in which shock waves are computed coming from the tip of the rod. Comparing

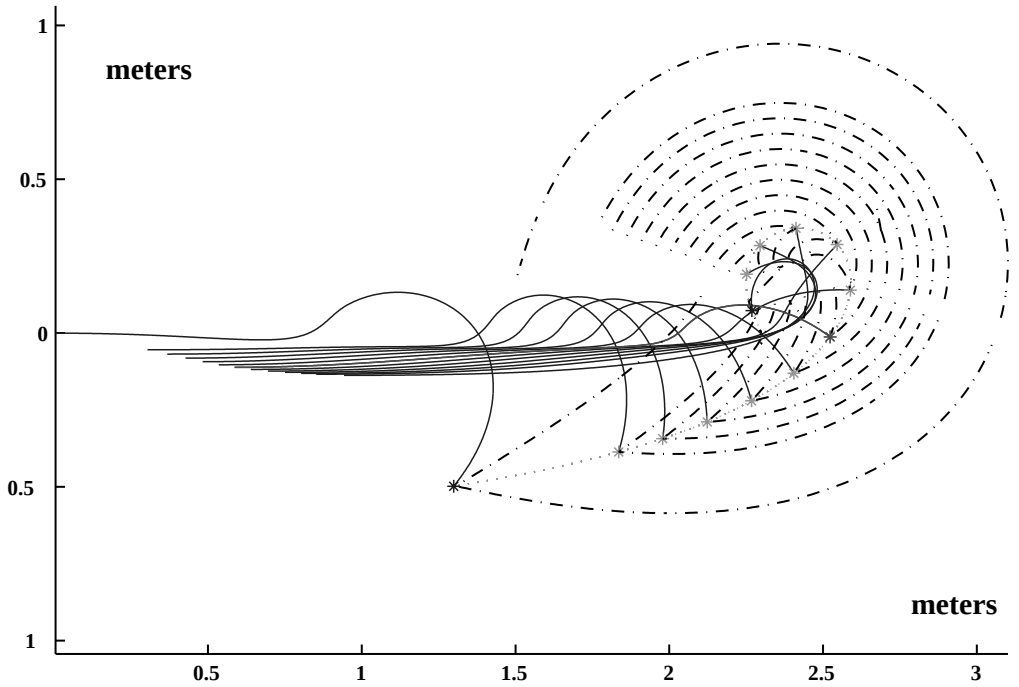

Fig. 20. Numerical solution in Case II at various times. The solid curves are the rod; the dashed curve is the path the tip of the whip travels; the dash-dotted curves are the shock waves.

this result to the photographs of Krehl et al. in Fig. 1, we see that the shock waves as computed from coming off of the curve the tip of the whip travels, are consistent with those photographed in actual whip cracks. This suggests that is, in fact, the tip of the whip, or a small section of the rod near the tip, that produces the crack.

8. Conclusions

As anybody who has cracked a whip can attest, producing a loud crack requires a subtle combination of motion to create an initial loop and let it travel along the whip to the end. Similarly, we found at the numerical level, that it takes a fair amount of experimenting with various boundary conditions, speeds and tensions, to find the correct parameters so that the tip accelerates sufficiently to produce a crack. The most efficient way to crack a whip, in terms of producing the loudest crack for the least amount of effort, is to send a planar loop down a tapering rod with extra applied tension to provide further acceleration. The same type of motion is found in fly-fishing where tension is used to optimize a throw [29].

The crack itself is a sonic boom created when a section of the whip at its tip travels faster than the speed of sound. The rapid acceleration of the tip of the whip is created when a wave travels to the end of the rod, and the energy consisting of the kinetic energy of the moving loop, the elastic energy stored in the loop, and the angular momentum of the rod is concentrated into a small section of the rod, which is then transferred into acceleration of the end of the rod.

Several factors combine to create a wave with a high speed as it travels to the end of the rod. Additional tension at the handle end, increasing the speed of the initial loop, and the tapering in the rod all serve to increase the maximum speed of the tip of the rod. The main effect seems to be the tapering in the rod, which increases the maximal speed

nonlinearly. Thus, the main key in successful whip cracking seems to be in the design of an efficient elastic tapered whip as both whip artists and craftspeople will tell you.

Acknowledgements

We thank Ph. Hanset, A. Ruina, and M. Tabor for discussions, and are indebted to A. Conway and P. Krehl for sharing their images of whips. TM is supported through the NSF-VIGRE initiative. AG is supported by the Sloan foundation and the NSF grant DMS9972063.

Appendix A. Numerical scheme

A.1. Proof of Lemma 6.1

Lemma A.1. *For every $n \geq 0$, we have $E_{n+1} = E_n + R_n$, where E_n is defined by (98), and R_n is given by*

$$\begin{aligned} R_n &= \tfrac{1}{2}[\delta^2_{N+1}\Delta^+_h\theta^n_N(\theta^{n+1}_N - \theta^{n-1}_N) - \delta^2_1\Delta^+_h\theta^n_0(\theta^{n+1}_0 - \theta^{n-1}_0) + f^n_N(x^{n+1}_{N+1} - x^{n-1}_{N+1}) - f^n_0(x^{n+1}_1 - x^{n-1}_1) \\ &\quad + g^n_N(y^{n+1}_{N+1} - y^{n-1}_{N+1}) - g^n_0(y^{n+1}_1 - y^{n-1}_1)]. \end{aligned} \tag{A.1}$$

Proof. We first multiply Eq. (83) by $\delta^2_j h(\theta^{n+1}_j - \theta^{n-1}_j)$, and sum from $j = 1$ to N. The left-hand side of the resulting equation is, after summing by parts the second term, and simplifying,

$$\begin{aligned} \mathrm{LHS} &= h\sum_{j=1}^N \delta^2_j(\Delta^+_\tau\theta^n_j)^2 - h\sum_{j=1}^N \delta^2_j(\Delta^+_\tau\theta^{n-1}_j)^2 + h\sum_{j=1}^N \delta^2_j\Delta^-_h\theta^{n+1}_j\Delta^-_h\theta^n_j - h\sum_{j=1}^N \delta^2_j\Delta^-_h\theta^n_j\Delta^-_h\theta^{n-1}_j \\ &\quad + h\sum_{j=1}^N \Delta^-_h\delta^2_j\Delta^-_h\theta^n_j(\theta^{n+1}_{j-1} - \theta^{n-1}_{j-1}) - \delta^2_N\Delta^+_h\theta^n_N(\theta^{n+1}_N - \theta^{n-1}_N) + \delta^2_0\Delta^+_h\theta^n_0(\theta^{n+1}_0 - \theta^{n-1}_0). \end{aligned} \tag{A.2}$$

For the right-hand side of the equation we use the fact

$$\cos\theta^{n+1}_j - \cos\theta^{n-1}_j = \frac{x^{n+1}_{j+1} - x^{n-1}_{j+1} - x^{n+1}_j + x^{n-1}_j}{h}, \tag{A.3}$$

and hence

$$\begin{aligned} h\sum_{j=1}^N f^n_j(\cos\theta^{n+1}_j - \cos\theta^{n-1}_j) &= \sum_{j=1}^N f^n_j(x^{n+1}_{j+1} - x^{n-1}_{j+1} - x^{n+1}_j + x^{n-1}_j) \\ &= -\sum_{j=1}^N (f^n_j - f^n_{j-1})(x^{n+1}_j - x^{n-1}_j) + f^n_N(x^{n+1}_{N+1} - x^{n-1}_{N+1}) - f^n_0(x^{n+1}_1 - x^{n-1}_1) \\ &= -h\sum_{j=1}^N \delta_j\Delta^2_\tau x^n_j(x^{n+1}_j - x^{n-1}_j) + f^n_N(x^{n+1}_{N+1} - x^{n-1}_{N+1}) - f^n_0(x^{n+1}_1 - x^{n-1}_1), \end{aligned} \tag{A.4}$$

and the fact that $\Delta^2_\tau x^n_j(x^{n+1}_j - x^{n-1}_j) = (\Delta^+_\tau x^n_j)^2 - (\Delta^+_\tau x^{n-1}_j)^2$, to compute

$$\begin{aligned}\text{RHS} = {} & h\sum_{j=1}^{N}\Delta_h^-\delta_j^2\Delta_h^-\theta_j^n(\theta_{j-1}^{n+1}-\theta_{j-1}^{n-1}) - h\sum_{j=1}^{N}\delta_j[(\Delta_\tau^+x_j^n)^2-(\Delta_\tau^+x_j^{n-1})^2]\\ & - h\sum_{j=1}^{N}\delta_j[(\Delta_\tau^+y_j^n)^2-(\Delta_\tau^+y_j^{n-1})^2] + h(\delta_{N+1}^2-\delta_N^2)\Delta_h^-\theta_{N+1}^n(\theta_N^{n+1}-\theta_N^{n-1})\\ & - h(\delta_1^2-\delta_0^2)\Delta_h^-\theta_1^n(\theta_0^{n+1}-\theta_0^{n-1}) + f_N^n(x_{N+1}^{n+1}-x_{N+1}^{n-1}) - f_0^n(x_1^{n+1}-x_1^{n-1})\\ & + g_N^n(y_{N+1}^{n+1}-y_{N+1}^{n-1}) - g_0^n(y_1^{n+1}-y_1^{n-1}). \end{aligned} \tag{A.5}$$

Comparing the RHS with the LHS, we see that the lemma holds. □

A.2. Case I numerics

We first describe the numerical scheme for Case I. Then we will describe how the scheme is modified for Cases II and III.

We start by solving (81) and (82) for f_j^n, g_j^n. Setting

$$A_{1,1} = -\frac{1}{h^2}\left(\frac{1}{\delta_1}+\frac{1}{\delta_2}\right), \qquad A_{1,2} = \frac{1}{h^2\delta_2}, \tag{A.6}$$

$$A_{j,j-1} = \frac{1}{h^2\delta_j}, \qquad A_{j,j} = -\frac{1}{h^2}\left(\frac{1}{\delta_j}+\frac{1}{\delta_{j+1}}\right), \qquad A_{j,j+1} = \frac{1}{h^2\delta_{j+1}} \quad \text{if } 1<j<N, \tag{A.7}$$

$$A_{N,1} = \frac{1}{h^2\delta_1}, \qquad A_{N,N-1} = \frac{1}{h^2\delta_N}, \tag{A.8}$$

$$A_{jN} = 1 \quad \text{for } 1\le j\le N, \tag{A.9}$$

$$A_{ij} = 0 \quad \text{otherwise}, \tag{A.10}$$

$$\mathbf{d} = \frac{1}{h^2}\left(\frac{1}{\delta_0}, 0, 0, \ldots, 0, \frac{1}{\delta_N}, -\left(\frac{1}{\delta_1}+\frac{1}{\delta_N}\right)\right)^{\mathrm{T}}, \tag{A.11}$$

and

$$A_{ij}^+ = (\mathbf{A}^{-1})_{ij} \quad \text{if } i<N, \quad A_{Nj}^+ = 0, \tag{A.12}$$

$$b_i = -(\mathbf{A}^{-1}\mathbf{d})_i \quad \text{if } i<N, \quad b_N = 1, \tag{A.13}$$

and letting $f_h^n = (f_1^n, f_2^n, \ldots, f_N^n)^{\mathrm{T}}$, and similarly for g_h^n, then (81) and (82) are solved by

$$f_h^n = \mathbf{b}\hat{f}^n + \mathbf{A}^+(\Delta_\tau^2\cos\theta_1^n, \Delta_\tau^2\cos\theta_2^n, \ldots, \Delta_\tau^2\cos\theta_N^n)^{\mathrm{T}}, \tag{A.14}$$

$$g_h^n = \mathbf{b}\hat{g}^n + \mathbf{A}^+(\Delta_\tau^2\sin\theta_1^n, \Delta_\tau^2\sin\theta_2^n, \ldots, \Delta_\tau^2\sin\theta_N^n)^{\mathrm{T}}, \tag{A.15}$$

where

$$\hat{f}^n = f_0^n = f_N^n, \qquad \hat{g}^n = g_0^n = g_N^n \tag{A.16}$$

with the compatibility condition

$$\Delta_\tau^2\sum_{j=1}^{N}\cos\theta_j^n = 0, \qquad \Delta_\tau^2\sum_{j=1}^{N}\sin\theta_j^n = 0. \tag{A.17}$$

In order to simplify notation, and conform to the notation in [43], we will call

$$\mathbf{c} = (\Delta_\tau^2 \cos\theta_1^n, \Delta_\tau^2 \cos\theta_2^n, \ldots, \Delta_\tau^2 \cos\theta_N^n)^{\mathrm{T}},$$
$$\mathbf{s} = (\Delta_\tau^2 \sin\theta_1^n, \Delta_\tau^2 \sin\theta_2^n, \ldots, \Delta_\tau^2 \sin\theta_N^n)^{\mathrm{T}}, \qquad \mathbf{K} = -\frac{1}{h}(\mathbf{A}^+)^{\mathrm{T}}. \tag{A.18}$$

We next make a few definitions to be used in the scheme.

$$\tilde{S}^n(\theta_j) = 2\int_0^L \int_0^L \xi \sin\left(\eta\xi\theta_j^{n+1} + (1-\eta)\xi\theta_j^n + (1-\xi)\theta_j^{n-1}\right) \mathrm{d}\eta\, \mathrm{d}\xi,$$
$$\tilde{C}^n(\theta_j) = 2\int_0^L \int_0^L \xi \cos\left(\eta\xi\theta_j^{n+1} + (1-\eta)\xi\theta_j^n + (1-\xi)\theta_j^{n-1}\right) \mathrm{d}\eta\, \mathrm{d}\xi,$$
$$\hat{S}^n(\theta_i, \theta_j) = -S^n(\theta_j)\tilde{C}^n(\theta_i) + C^n(\theta_j)\tilde{S}^n(\theta_i), \qquad \hat{C}^n(\theta_i, \theta_j) = S^n(\theta_j)S^n(\theta_i) + C^n(\theta_j)C^n(\theta_i). \tag{A.19}$$

Next, we use the solution for f, g, to form a single semi-linear equation for θ. Substituting (A.14) and (A.15) into (83), we have

$$\Delta_\tau^2\theta_j^n - \Delta_h^2\theta_j^n = \frac{1}{\delta_j^2}\Delta_h^+\delta_j^2\Delta_h^+\theta_j^n + \frac{\mathbf{b}_j}{\delta_j^2}[-\hat{f}^n S^n(\theta_j) + \hat{g}^n C^n(\theta_j)] + \frac{1}{\delta_j^2}[-(\mathbf{A}^+\mathbf{c})_j S^n(\theta_j) + (\mathbf{A}^+\mathbf{s})_j C^n(\theta_j)]. \tag{A.20}$$

A simple calculation shows that

$$c_j = \Delta_\tau^2 \cos\theta_j^n = -S^n(\theta_j)\Delta_\tau^2\theta_j^n - \tilde{C}^n(\theta_j)\Delta_\tau^+\theta_j^n\Delta_\tau^+\theta_j^{n-1}, \tag{A.21}$$

$$s_j = \Delta_\tau^2 \sin\theta_j^n = C^n(\theta_j)\Delta_\tau^2\theta_j^n - \tilde{S}^n(\theta_j)\Delta_\tau^+\theta_j^n\Delta_\tau^+\theta_j^{n-1}. \tag{A.22}$$

Another calculation shows

$$\frac{1}{\delta_j^2}[-(\mathbf{A}^+\mathbf{c})_j S^n(\theta_j^n) + (\mathbf{A}^+\mathbf{s})_j C^n(\theta_j^n)] = \frac{h}{\delta_j^2}\left[-\sum_{i=1}^N K_{ij}\hat{C}^n(\theta_i, \theta_j)\Delta_\tau^2\theta_i^n + \sum_{i=1}^N K_{ij}\hat{S}^n(\theta_i, \theta_j)\Delta_\tau^+\theta_i^n\Delta_\tau^+\theta_i^{n-1}\right]. \tag{A.23}$$

Substitution into (A.20) yields

$$\Delta_\tau^2\theta_j^n - \Delta_h^2\theta_j^n + \frac{h}{\delta_j^2}\sum_{i=1}^N K_{ij}\hat{C}^n(\theta_i, \theta_j)(\Delta_\tau^2\theta_i^n - \Delta_h^2\theta_i^n) = B^n(\theta_h)_j + \frac{\mathbf{b}_j}{\delta_j^2}[-\hat{f}^n S^n(\theta_j) + \hat{g}^n C^n(\theta_j)], \tag{A.24}$$

where

$$B^n(\theta_h)_j = \frac{1}{\delta_j^2}\Delta_h^+\delta_j^2\Delta_h^+\theta_j^n + \frac{h}{\delta_j^2}\sum_{i=1}^N K_{ij}\hat{S}^n(\theta_i, \theta_j)\Delta_\tau^+\theta_i^n\Delta_\tau^+\theta_i^{n-1} - \frac{h}{\delta_j^2}\sum_{i=1}^N K_{ij}\hat{C}^n(\theta_i, \theta_j)\Delta_h^2\theta_i^n. \tag{A.25}$$

Summation by parts shows that

$$h\sum_{i=1}^{N} K_{ij}\hat{C}^n(\theta_i,\theta_j)\Delta_h^2\theta_i^n = -\sum_{i=2}^{N}(K_{ij}\hat{C}^n(\theta_i,\theta_j) - K_{i-1,j}\hat{C}^n(\theta_{i-1},\theta_j))\Delta_h^-\theta_i^n + \frac{1}{h}\left(\frac{\delta_0^2}{\delta_N^2}K_{Nj}\hat{C}^n(\theta_N,\theta_j) - K_{1j}\hat{C}^n(\theta_1,\theta_j)\right)(\theta_1^n - \theta_N^n + 2\pi k). \tag{A.26}$$

Therefore,

$$B^n(\theta_h)_j = \frac{1}{\delta_j^2}\Delta_h^+\delta_j^2\Delta_h^+\theta_j^n + \frac{h}{\delta_j^2}\sum_{i=1}^{N} K_{ij}\hat{S}^n(\theta_i,\theta_j)\Delta_\tau^+\theta_i^n\,\Delta_\tau^+\theta_i^{n-1} + \frac{1}{\delta_j^2}\sum_{i=2}^{N}(K_{ij}\hat{C}^n(\theta_i,\theta_j) - K_{i-1,j}\hat{C}^n(\theta_{i-1},\theta_j))\Delta_h^-\theta_i^n - \frac{1}{h\delta_j^2}\left(\frac{\delta_0^2}{\delta_N^2}K_{Nj}\hat{C}^n(\theta_N,\theta_j) - K_{1j}\hat{C}^n(\theta_1,\theta_j)\right)(\theta_1^n - \theta_N^n + 2\pi k). \tag{A.27}$$

We are thus able to form the semi-linear equation. Setting

$$(L_{\theta_h})_{ij} = \frac{h}{\delta_j^2}K_{ji}\hat{C}^n(\theta_j,\theta_i), \tag{A.28}$$

$$A^n(\theta_h)_j = \frac{\mathbf{b}_j}{\delta_j^2}[-\hat{f}^n S^n(\theta_j^n) + \hat{g}^n C^n(\theta_j^n)] + B^n(\theta_h)_j, \tag{A.29}$$

Eq. (A.20) is equivalent to

$$\Delta_\tau^2\theta_h^n - \Delta_h^2\theta_h^n = (\mathbf{I} + \mathbf{L}_{\theta_h})^{-1}A^n(\theta_h). \tag{A.30}$$

Eq. (A.30) is a semi-linear equation. In order to form a semi-linear equation for θ only, we next solve for $\hat{f}^n$, $\hat{g}^n$. Let

$$Sb^n(\theta_j) = \frac{b_j}{\delta_j^2}S^n(\theta_j), \tag{A.31}$$

$$Cb^n(\theta_j) = \frac{b_j}{\delta_j^2}C^n(\theta_j). \tag{A.32}$$

Multiplying (A.30) by $S^n(\theta_h)^{\mathrm{T}}$ and $C^n(\theta_h)^{\mathrm{T}}$, respectively, and summing by parts, assuming the compatibility condition (A.17), the following relations hold:

$$a_{11}(\theta_h)\hat{f}^n + a_{12}(\theta_h)\hat{g}^n = \sum_{j=1}^{N}\tilde{C}^n(\theta_j)\Delta_\tau^+\theta_j^n\,\Delta_\tau^+\theta_j^{n-1} - \sum_{j=1}^{N}\tilde{D}_h^- S^n(\theta_j)\Delta_h^-\theta_j^n + S^n(\theta_h)^{\mathrm{T}}(\mathbf{I} + \mathbf{L}_{\theta_h})^{-1}B^n(\theta_h), \tag{A.33}$$

$$a_{21}(\theta_h)\hat{f}^n + a_{22}(\theta_h)\hat{g}^n = -\sum_{j=1}^{N}\tilde{S}^n(\theta_j)\Delta_\tau^+\theta_j^n\,\Delta_\tau^+\theta_j^{n-1} - \sum_{j=1}^{N}\tilde{D}_h^- C^n(\theta_j)\Delta_h^-\theta_j^n + C^n(\theta_h)^{\mathrm{T}}(\mathbf{I} + \mathbf{L}_{\theta_h})^{-1}B^n(\theta_h), \tag{A.34}$$

where

$$\tilde{D}_h^- u_j = \frac{u_j - u_{j-1}}{h} \quad \text{if } 2 \le j \le N, \tag{A.35}$$

$$\tilde{D}_h^- u_1 = \frac{u_1 - (\delta_0^2/\delta_N)^2 u_N}{h}, \tag{A.36}$$

and

$$a_{11}(\theta_h) = S^n(\theta_h)^{\mathrm{T}}(\mathbf{I} + \mathbf{L}_{\theta_h})^{-1} S b^n(\theta_h), \tag{A.37}$$

$$a_{12}(\theta_h) = -S^n(\theta_h)^{\mathrm{T}}(\mathbf{I} + \mathbf{L}_{\theta_h})^{-1} C b^n(\theta_h), \tag{A.38}$$

$$a_{21}(\theta_h) = C^n(\theta_h)^{\mathrm{T}}(\mathbf{I} + \mathbf{L}_{\theta_h})^{-1} S b^n(\theta_h), \tag{A.39}$$

$$a_{22}(\theta_h) = -C^n(\theta_h)^{\mathrm{T}}(\mathbf{I} + \mathbf{L}_{\theta_h})^{-1} C b^n(\theta_h). \tag{A.40}$$

Thus, if we assume a priori that (A.33) and (A.34) hold, then the compatibility condition (A.17) is automatically satisfied. Thus, we solve for $\hat{f}^n$, $\hat{g}^n$, and substitute the result into (A.30), then we have a semilinear equation for θ only.

Accordingly, we form the semilinear equation for θ, and solve for θ^{n+1} iteratively. Letting

$$G^n(\theta_h^{n+1}, \theta_h^n, \theta_h^{n-1}) = (\mathbf{I} + \mathbf{L}_{\theta_h})^{-1} A^n(\theta_h), \tag{A.41}$$

we define the iteration:

$$\frac{1}{\tau^2}(\theta_h^{n+1,k+1} - 2\theta_h^n + \theta_h^{n-1}) - \Delta_h^2 \theta_h^n = G^n(\theta_h^{n+1,k}, \theta_h^n, \theta_h^{n-1}), \tag{A.42}$$

$$\theta_h^{n+1,0} = 2\theta_h^n - \theta_h^{n-1}. \tag{A.43}$$

We iterate until $\|\theta_h^{n+1,k+1} - \theta_h^{n+1,k}\| < \text{tol}$, where tol is typically 10^{-8}. Once θ_j^n has been calculated, f_j^n, g_j^n are defined by (A.14) and (A.15), and x_j^n, y_j^n by (88) and (89). All that remains is to calculate x_a^n and y_a^n. These must satisfy

$$\Delta_\tau^2 x_a^n = \frac{1}{\delta_1} \Delta_h^- f_1^n, \tag{A.44}$$

$$\Delta_\tau^2 y_a^n = \frac{1}{\delta_1} \Delta_h^- g_1^n. \tag{A.45}$$

The set of equations (A.44) and (A.45) forms a linear system, which we solve by Gaussian elimination, after the calculation of all the θ_j^n. There is still one degree of freedom, in which one can add a line to the solution, corresponding to moving the inertial frame of reference.

A.3. Case II numerics

In Case II, we can solve for f_h^n, g_h^n, with the boundary conditions in (95), directly by inverting a matrix, as there is no compatibility condition. We solve for f_h and g_h in (A.14) and (A.15) by setting

$$\tilde{f}_h^n = (f_1, f_2, \ldots, f_{N-1}, f_{N+1}), \tag{A.46}$$

and similarly for $\tilde{g}_h^n$. Then $\tilde{f}_h^n$ and $\tilde{g}_h^n$ are solved by

$$\tilde{f}_h^n = \mathbf{A}^{-1}(\Delta_\tau^2 \cos\theta_1^n - \frac{\alpha}{h^2\delta_1}, \Delta_\tau^2 \cos\theta_2^n, \ldots, \Delta_\tau^2 \cos\theta_N^n)^{\mathrm{T}}, \tag{A.47}$$

$$\tilde{g}_h^n = \mathbf{A}^{-1}(\Delta_\tau^2 \sin\theta_1^n, \Delta_\tau^2 \sin\theta_2^n, \ldots, \Delta_\tau^2 \sin\theta_N^n)^{\mathrm{T}}, \tag{A.48}$$

where $\mathbf{A}$ is now

$$A_{1,1} = -\frac{1}{h^2}\left(\frac{1}{\delta_1} + \frac{1}{\delta_2}\right), \qquad A_{1,2} = \frac{1}{h^2\delta_2}, \tag{A.49}$$

$$A_{j,j-1} = \frac{1}{h^2\delta_j}, \qquad A_{j,j} = -\frac{1}{h^2}\left(\frac{1}{\delta_j} + \frac{1}{\delta_{j+1}}\right), \qquad A_{j,j+1} = \frac{1}{h^2\,\delta_{j+1}} \quad \text{if } 1 < j < N, \tag{A.50}$$

$$A_{N-1,N} = 0, \qquad A_{N,N-1} = \frac{1}{\delta_N}, \qquad A_{N,N} = \frac{1}{\delta_{N+1}}, \tag{A.51}$$

$$A_{ij} = 0 \quad \text{otherwise.} \tag{A.52}$$

We can thus take $\mathbf{A}^+ = \mathbf{A}^{-1}$. Then, $\mathbf{b}$ and $\mathbf{c}$ in (A.18) are changed by

$$\mathbf{b} \to 0, \tag{A.53}$$

$$\mathbf{c} \to \mathbf{c} - \left(\frac{\alpha}{h^2\delta_1}, 0, \ldots, 0\right), \tag{A.54}$$

and $\mathbf{K} = -(1/h)(\mathbf{A}^{-1})^{\mathrm{T}}$. We must also change the derivatives of θ at $j = 1, N$ to correspond with the boundary conditions (95). In particular,

$$\Delta_h^- \theta_1^n = \frac{\theta_1^n}{h}, \qquad \Delta_h^+ \theta_N^n = 0. \tag{A.55}$$

Making these changes, we see that

$$\begin{aligned} A^n(\theta_h)_j = {} & \frac{1}{\delta_j^2}\Delta_h^+\delta_j^2\Delta_h^+\theta_j^n + \frac{h}{\delta_j^2}\sum_{i=1}^{N} K_{ij}\hat{S}^n(\theta_i,\theta_j)\Delta_\tau^+\theta_i^n\,\Delta_\tau^+\theta_i^{n-1} \\ & + \frac{1}{\delta_j^2}\sum_{i=2}^{N}(K_{ij}\hat{C}^n(\theta_i,\theta_j) - K_{i-1,j}\hat{C}^n(\theta_{i-1},\theta_j))\Delta_h^-\theta_i^n \\ & - \frac{K_{1j}}{h\delta_j^2}\left(\frac{\alpha}{\delta_1}S^n(\theta_j) - \hat{C}^n(\theta_1,\theta_j)\theta_1^n\right), \qquad A^n(\theta_h)_N = 0. \end{aligned} \tag{A.56}$$

Then the iteration (A.42) and (A.43) with the relation (A.41) will solve Case II.

A.4. Case III numerics

The difference between Cases II and III is in the condition at the left end. In Case III the left end is held fixed. This means that the tension at the left end varies as a function of time, rather than being fixed, as in Case II. Note that the condition $x_a^n = y_a^n = 0$ is equivalent to the condition

$$\Delta_h^- f_1^n = \Delta_h^- g_1^n = 0. \tag{A.57}$$

Therefore, $f_0^n = f_1^n$ and $g_0^n = g_1^n$. And since $f_N^n = g_N^n = 0$, we only need to solve for f_j^n, g_j^n for $1 \le j \le N-1$ and $i = N+1$ as in Case II. We thus solve for $\tilde{f}_h^n$ and $\tilde{g}_h^n$ as in Case II, by making the following change in **A**, in addition to those in Case II:

$$A_{1,1} \to -\frac{1}{h^2\delta_2}. \tag{A.58}$$

The solution for $\tilde{f}_h^n, \tilde{g}_h^n$ are then given by

$$\tilde{f}_h^n = \mathbf{A}^{-1}(\Delta_\tau^2 \cos\theta_1^n, \Delta_\tau^2 \cos\theta_2^n, \ldots, \Delta_\tau^2 \cos\theta_N^n)^{\mathrm{T}}, \tag{A.59}$$

$$\tilde{g}_h^n = \mathbf{A}^{-1}(\Delta_\tau^2 \sin\theta_1^n, \Delta_\tau^2 \sin\theta_2^n, \ldots, \Delta_\tau^2 \sin\theta_N^n)^{\mathrm{T}}. \tag{A.60}$$

The calculation in Case III then proceeds as in Case II. With these changes, $A^n(\theta_h)$ is as in (A.56) with $\alpha \to 0$.

A.5. Case IV numerics

Case IV proceeds as in Case III, but with $\theta_0^n = \theta_1^n$, and we only need to change the definition of the discrete derivative $\Delta_h^- \theta_1^n$, wherever it occurs.

A.6. Scaling—implementation of the scheme

In the actual computation, the length of the filament is scaled out. This is necessary in order to run a realistic simulation, since L may be very large. For example, a 3 m long rod with a 2 cm typical radius, $L = 300$. Since h must be on the order of 10^{-2} in order for the iteration to converge, we would have to take make the number of spatial steps $N = 30{,}000$, far too large to run a simulation in a lifetime. We thus scale the length of the filament as follows:

$$s \to \frac{s}{L}, \qquad t \to \frac{t}{L}. \tag{A.61}$$

We can then take the discrete space step $h = 1/N$. The equations for the linear momenta (14) and (15) and (81) and (82) remain unchanged, but the moment equations (16) and (83) are changed by

$$F, G \to L^2(F, G) \tag{A.62}$$

with the corresponding changes made in the discretized equations (see [44] for details on the changes to the scheme with this scaling). With this scaling, we can take the number of space steps to be on the order of 10^2 in order to obtain convergence, a number that allows for computation in a reasonable amount of time.

References

[1] D. Morgan, Whips and Whipmaking, Cornell Maritime Press, Centerville, MD, 1972.
[2] M. Allen, The Art of the Bullwhip, Mark Allen Productions, Las Vegas, 1989.
[3] R. Edwards, How to Make a Whip, Cornell Maritine Press, Centerville, MD, 1997.
[4] P. Krehl, S. Engemann, D. Schwenkel, The puzzle of whip cracking—uncovered by a correlation of whip-tip kinematics with shock wave emission, Shock Waves 8 (1998) 1–9.
[5] O. Lummer, Über die Theorie des Knalls, Schlesische Gesellschaft für vaterländische Kultur 83 (1905) 2.
[6] Editorial, Why a whip "cracks", Sci. Am. (April 3, 1915).
[7] J.M. Jones, The crack of a whip, Sci. Am. (July 10, 1915) 43.
[8] E.E. Larson, Why a whip cracks, Sci. Am. (July 24, 1915).
[9] H.P. Maxim, The whiplash crack and bullet sound waves, Sci. Am. (September 11, 1915) 231.

[10] L. Prandtl, Gasbewegung, Handẅorterbuch der Naturwissenschaften 4 (1013) 454.
[11] W. Bragg, The World of Sound, Dover, New York, 1968.
[12] Z. Carrière, Le claquement du fouet, J. Phys. Radium Ser. VI 8 (1927) 365–384.
[13] Z. Carrière, Exploration par le fouet des deux faces du mur du son, Cahiers de Physique 63 (1955) 1–17.
[14] B. Bernstein, D.A. Hall, H.M. Trent, On the dynamics of a bull whip, J. Acoust. Soc. Am. 30 (1958) 1112–1115.
[15] N.P. Myrhvold, P.J. Curie, Supersonic sauropods? Tail dynamics in the diplodocids, Paleobiology 23 (1997) 393–409.
[16] W. Kucharski, Zur Kinetikdehnungsloser Seile mit Knickstellen, Ing. Arch. 12 (1941) 109–123.
[17] R. Grammel, K. Zoller, Zur Mechanik der Peitsche und des Peitschenknalles, Z. Phys. 127 (1949) 11–15.
[18] W. Burger, Peitschenknall mit Überschal, Bild der Wissenschaft, August 1995, pp. 102–103.
[19] W. Steiner, H. Troger, On the equations of motion of the folded inextensible string, ZAMP 46 (1995) 960–970.
[20] M. Zak, J.P. Zbilut, R.E. Meyers, From Instability to Intelligence, Springer, New York, 1997.
[21] A. Conway, The Bullwhip Book, Greenery Press, Emeryville, CA, 2000.
[22] R.S. Johnson, On the development of a solitary wave moving over uneven bottom, Proc. Camb. Philos. Soc. 73 (1973) 183–203.
[23] R. Grimshaw, Slowly varying solitary waves. I. Korteweg–de Vries equation, Proc. R. Soc. London A 368 (1979) 359–375.
[24] C.J. Knickerbocker, A.C. Newell, Shelves and the Korteweg–de Vries equation, J. Fluid. Mech. 98 (1980) 803–818.
[25] T. Warn, The evolution of finite amplitude solitary Rosby waves on a weak shear, Stud. Appl. Math. 69 (1983) 127–133.
[26] A.M. Samsonov, Evolution of a soliton in a nonlinearly elastic rod of variable cross section, Sov. Phys. Dokl. 29 (1984) 586–587.
[27] D. Prasad, T.R. Akylas, On the generation of shelves by long linear waves in stratified flows, J. Fluid. Mech. 246 (1997) 245–262.
[28] A.M. Samsonov, S.V. Dreiden, A.V. Porubov, I.V. Semenova, Longitudinal-strain soliton focusing in a narrowing nonlinear elastic rod, Phys. Rev. B 57 (1998) 5778–5787.
[29] G.A. Spolek, The mechanics of flycasting: the flyline, Am. J. Phys. 54 (1986) 832–835.
[30] C. Gatti, N.C. Perkins, Numerical analysis of flycasting mechanics, BED-Bioeng. Conf. ASME 50 (2001) 277–278.
[31] D. Reinhart, J. Ridgway, D.E. Chandler, Xenopus laevis fertilisation: analysis of sperm motility in egg jelly using light video microscopy, Zygote 6 (1998) 173–182.
[32] R.E. Caflish, J.H. Maddocks, Nonlinear dynamical theory of the elastica, Proc. R. Soc. Edinburgh A 99 (1984) 1–23.
[33] S.S. Antman, Nonlinear Problems of Elasticity, Springer, New York, 1995.
[34] M.F. Ashby, L.J. Gibson, U. Wegst, R. Olive, The mechanical properties of natural materials. I. Material property charts, Proc. R. Soc. London A 450 (1995) 123–140.
[35] N. Lee, S. Allen, E. Smith, L.W. Winters, Does the tip of a snapped towel travel faster than sound?, Phys. Teach. 31 (1993) 376–377.
[36] D. Struik, Lectures on Classical Differential Geometry, Dover, Toronto, 1988.
[37] B.D. Coleman, E.H. Dill, M. Lembo, Z. Lu, I. Tobias, On the dynamics of rods in the theory of Kirchhoff and Clebsch, Arch. Rat. Mech. Anal. 121 (1993) 339–359.
[38] R.S. Falk, J.M. Xu, Convergence of a second-order scheme for the nonlinear dynamical equations of elastic rods, SIAM J. Numer. Anal. 32 (1995) 1185–1209.
[39] J.H. Maddocks, D.J. Dichmann, Conservation laws in the dynamics of rods, J. Elasticity 34 (1994) 83–96.
[40] B.D. Coleman, E.H. Dill, Flexure waves in elastic rods, J. Acoust. Soc. Am. 91 (1992) 2663.
[41] B.D. Coleman, E.H. Dill, D. Swigon, On the dynamics of flexure and stretch in the theory of elastic rods, Arch. Rat. Mech. Anal. 129 (1995) 147–174.
[42] R. Grimshaw, H. Mitsudera, Slowly varying solitary wave solutions of the perturbed Korteweg–de Vries equation revisited, Stud. Appl. Math. 90 (1993) 75–86.
[43] B.D. Coleman, J.M. Xu, On the interaction of solitary waves of flexure in elastic rods, Acta Mech. 110 (1995) 173–182.
[44] J.M. Xu, An analysis of the dynamical equations of elastic rods and their numerical approximation, Ph.D. Dissertation, Rutgers University, New Brunswick, May 1992.
[45] E. Isaacson, H.B. Keller, Analysis of Numerical Methods, Dover, New York, 1994.
[46] C.V. Boys, Soap bubbles; their colours and the forces which mould them, being the substance of many lectures delivered to juvenile and popular audiences with an addition of several new and original sections, Society for Promoting Christian Knowledge, London, Macmillan, New York, 1924.